공학박사 학위논문

Methane Dehydro-aromatization over Mo-based catalysts

몰리브데넘 기반 촉매를 이용한 메탄 탈수소 방향족화 반응

2023년 8월

서울대학교 대학원

화학생물공학부

남 기 훈

Methane Dehydro-aromatization over Mo-based catalysts

지도 교수 김 도 희

이 논문을 공학박사 학위논문으로 제출함
2023년 7월

서울대학교 대학원
화학생물공학부
남 기 훈

남기훈의 공학박사 학위논문을 인준함
2023년 7월

위 원 장 _____ 이 원 보 _____ (인)

부위원장 _____ 김 도 희 _____ (인)

위 원 _____ 강 종 헌 _____ (인)

위 원 _____ 김 지 만 _____ (인)

위 원 _____ 박 영 권 _____ (인)

Abstract

Benzene, toluene, and xylene (BTX) are essential chemicals used as feedstocks in various industries, including plastics, rubber, textiles, pharmaceuticals, and paints. The global demand for BTX is expected to continue to grow due to increasing population, urbanization, and industrialization. Nevertheless, the production of BTX is significantly reliant on crude oil. Natural gas, mainly consists of methane, is recognized as good alternative carbon source that can replace crude oil, as it has abundant reserves and environmentally friendliness. Therefore, BTX production process using methane is considered an economically and environmentally important process.

However, methane utilization is challenging because of the high C-H activation energy of methane. The route for utilizing methane is divided into indirect conversion, and direct conversion. In indirect conversion, methane is converted into syngas via reaction, such as steam reforming or partial oxidation; and then other hydrocarbons are produced from the syngas, via the Fischer–Tropsch process or methanol synthesis. Such multi-step process results in high energy consumption. In contrast, by eliminating the intermediate syngas generation step, direct conversion has both energetic and economic advantages. Direct conversion can be classified into oxidative reaction and non-oxidative reaction. Oxidative reaction can increase the reactivity of methane, although most methane is completely oxidized to CO_2

and H_2O. Therefore, non-oxidative reaction is considered a more appropriate approach to increase the selectivity of the desired product. In these reasons, methane dehydro-aromatization (MDA) is one of the most attractive process.

While Mo/HZSM-5 is known as a catalyst for MDA, low activity and rapid deactivation have been considered issues to be overcome. In order to improve catalytic performance, NiO was physically mixed with Mo/HZSM-5, which significantly enhanced the yield for aromatic compounds (benzene and toluene), and improved catalytic stability. Also, effects of additional silica shells on NiO ($NiO@SiO_2$) and NiO/SiO_2 ($SiO_2@NiO/SiO_2$) were confirmed. Combined X-ray diffraction (XRD), CH4-temperature programmed surface reaction (CH4–TPSR), CO chemisorption, transmission electron microscopy coupled with energy dispersive spectroscopy (TEM-EDS), temperature programmed oxidation (TPO), visible Raman, and N_2 physisorption analysis confirmed that NiO promoted the dispersion of MoCx active sites and suppressed coke formation on MoCx, by converting coke precursors to carbon nanotube (CNT) on itself. As a result, after the reaction, the pore size and pore volume did not change much, which is attributed to the improved stability.

In addition, the presence of silica shells on NiO was also found to promote MoCx dispersion by altering activation temperature of MoCx, but the shells were broken, resulting in the formation of CNTs similarly to bare NiO. In the case of silica shells on NiO/SiO_2 also, the catalytic activity was enhanced by lowering the activation temperature of MoCx. On the contrary,

metallic Ni exposure did not occur as much as bare NiO, resulting in less formation of CNTs, a different deactivation trend was observed. In conclusion, this study demonstrates that physically mixed NiO and silica coated NiO species can act as an excellent catalyst promotor for MDA.

Keyword : Methane dehydro-aromatization (MDA), Mo-based catalysts, Mo/HZSM-5, NiO, Physical mixing, Silica shell
Student Number : 2016-21024

Table of Contents

List of Tables

List of Figures

Chapter 1. Introduction

1.1. Study Background

Natural gas or shale gas, which is mainly composed of methane, is promising alternative carbon source which can replace petroleum in the industry (Fig. 1-1) [1]. During combustion, it emits primarily carbon dioxide and water vapors, while coal and oil produce complex molecules containing high contents of nitrogen and sulfur, which give rise to the environmental pollution [2]. Considering the emission during the utilization, methane is the cleanest and most environmentally benign fossil fuel [2, 3]. Therefore, it is more environmentally friendly if the chemicals produced from fossil fuels can be obtained from methane. Besides, natural gas or shale gas is generally transported through pipelines, or in the form of liquefied natural gas (LNG). However, pipelines need expensive construction costs, and present the danger of leaks. Also, as shown in Fig. 1-2, Fugitive emissions of natural gas or shale gas during transportation are extremely concerned because of powerful greenhouse gas effect of methane [4]. Therefore, it is desirable to develop an efficient process to convert methane into more valuable hydrocarbon products, not only in terms of methane utilization, but also in terms of environmental friendliness [5].

However, methane utilization is challenging because of the high C-H activation energy of methane. The route for utilizing methane is divided into indirect conversion, and direct conversion. In indirect conversion, methane is

converted into syngas via reaction, such as steam reforming or partial oxidation; and then other hydrocarbons are produced from the syngas, via the Fischer–Tropsch process or methanol synthesis [6]. Such multi-step process results in high energy consumption. In contrast, by eliminating the intermediate syngas generation step, direct conversion has both energetic and economic advantages [7]. Direct conversion can be classified into oxidative reaction and non-oxidative reaction. Oxidative reaction can increase the reactivity of methane, although most methane is completely oxidized to CO_2 and H_2O [8]. Therefore, non-oxidative reaction is considered a more appropriate approach to increase the selectivity of the desired product. Among the alternative reactions, methane dehydro-aromatization (MDA) is one of the most attractive, because value-added chemicals, such as benzene, toluene, and xylene (BTX), are obtained as products, and can be used as feedstock chemicals in industry (Fig. 1-3) [9]. In addition, hydrogen, which is an essential feedstock for chemical industry, is produced with BTX during MDA.

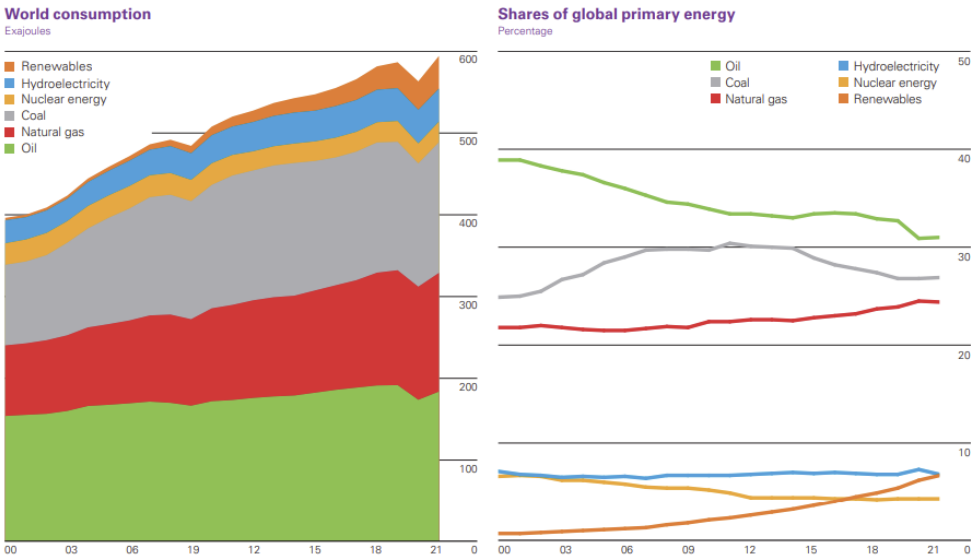

Fig 1-1. World energy consumption and shares of global primary energy.

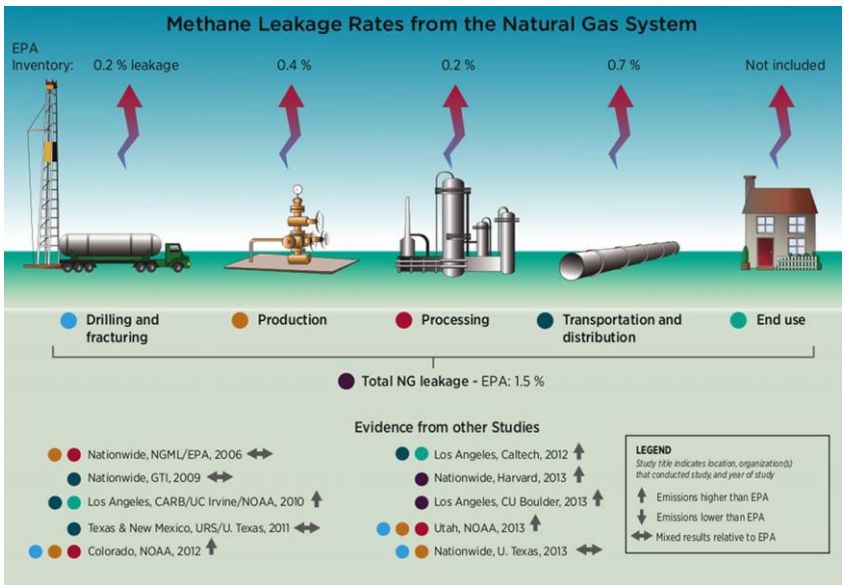

Fig 1-2. Methane leakage rates from the natural gas system.

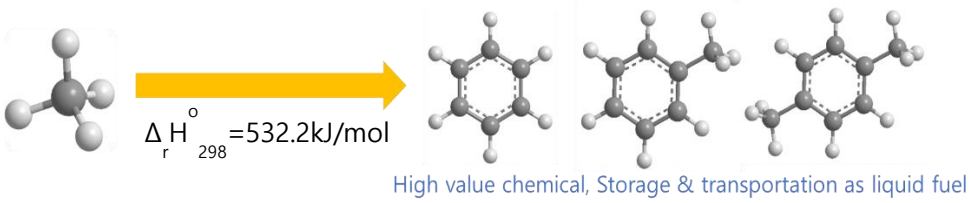

Fig 1-3. The scheme of methane dehydro-aromatization.

1.2. Methane dehydro-aromatization

Since Wang et al. first reported the MDA reaction for the production of benzene and hydrogen over Mo oxide supported on HZSM-5 (Mo/HZSM-5) at 700 °C [10], various metals supported on zeolite catalysts have been tested [11]. Previous studies concluded that the most promising catalysts for MDA were Mo supported on zeolites with pore diameters of 5–6 Å, such as ZSM-5, MCM-22, and ZSM-11 [12, 13]. The MDA reaction mechanism on Mo/HZSM-5 was reported to begin with carburization of the supported Mo oxide to Mo oxycarbide or Mo carbide (MoCx) during the reaction [14, 15]. The Mo carbide species activates the C–H bond of methane, which is the rate determining step of MDA [16, 17]. C_2 intermediates derived from the activation of methane are oligomerized, to produce products such as benzene. During the MDA reaction, coke is also formed via additional reaction in the intermediate state, or excessive oligomerization in the product-like state [18]. The formation of coke, unwanted carbonaceous deposit, causes rapid deactivation of the Mo/HZSM-5 catalyst. In particular, the polyaromatic coke formed on the external surface of the zeolite has been regarded as the main deactivation factor among various carbonaceous deposits [19]. Therefore, the major issue in MDA reaction lies in how to increase methane activity, and prevent rapid deactivation arising from coke formation.

In order to improve the methane activity, as well as to inhibit

deactivation, various approaches, such as promotor addition and pretreatment, have been undertaken. Although there are conflicting results among the research groups, the performance of the catalyst was enhanced when Fe [20, 21], Co [22, 23], Ni [24], Zn [21], Ga [25, 26], Ag [27], and P [28] were added as promotor. Tan showed that it was possible to increase the benzene yield and stability of Mo/HZSM-5 catalyst by using reaction gas (CH_4) during the pretreatment process [29]. In addition, metallic Ni has also been reported to have excellent methane dissociation ability [30].

1.3. Purpose of Research

In this study, NiO, silica coated NiO (NiO@SiO_2), and silica coated NiO/SiO_2 (SiO_2@NiO/SiO_2) were selected as a promoters, with anticipation that it could be converted to metallic Ni through the pretreatment process, which was expected to help methane activation. An earlier study reported that sequentially impregnated Ni-Mo/ZSM-5 increased catalytic activity and stability, because Ni prevents the sublimation of Mo species [31]. For comparison, we prepared Mo/HZSM-5 samples physically mixed with NiO, followed by reductive pretreatment. We found that physically mixed catalysts showed better catalytic performance and stability than the impregnated one. In addition, there is a previous study by Vosmerikov et al. who promoted catalytic activity with Ni addition via physical mixing [24]. However, they used the catalysts prepared by mechanically mixing Mo and Ni nano-sized powders with ZSM-5, not physical mixing of NiO and Mo/HZSM-5 like our study [24]. In this work, the catalytic performance of Mo/HZSM-5 catalyst was enhanced by the use of bulk NiO, which is superior with respect to the simplicity and cost of synthesis procedure. In particular, we further tried to elucidate the role of Ni in enhancing the activity and stability of MDA by investigating the physicochemical properties of the post-reaction samples. Furthermore, this study aims to provide better understanding of the underlying Mo active site activation and catalyst deactivation mechanism by investigating the changes in the activity and stability of the MDA reaction with physically mixing silica shell coated NiO(NiO@SiO_2) and NiO/SiO_2

(SiO_2@NiO/SiO_2) as promoters.

Chapter 2. Enhanced reactivity and stability in methane dehydro−aromatization over Mo/H ZSM−5 physically mixed with NiO

2.1. Introduction

Natural gas or shale gas, which is mainly composed of methane, is promising alternative carbon source which can replace petroleum in the industry [1]. During combustion, it emits primarily carbon dioxide and water vapors, while coal and oil produce complex molecules containing high contents of nitrogen and sulfur, which give rise to the environmental pollution [2]. Considering the emission during the utilization, methane is the cleanest and most environmentally benign fossil fuel [2, 3]. Therefore, it is more environmentally friendly if the chemicals produced from fossil fuels can be obtained from methane. Besides, natural gas or shale gas is generally transported through pipelines, or in the form of liquefied natural gas (LNG). However, pipelines need expensive construction costs, and present the danger of leaks. Fugitive emissions of natural gas or shale gas during transportation are extremely concerned because of powerful greenhouse gas effect of methane [4]. Therefore, it is desirable to develop an efficient process to convert methane into more valuable hydrocarbon products, not only in terms of methane utilization, but also in terms of environmental friendliness [5].

However, methane utilization is challenging because of the high C-H activation energy of methane. The route for utilizing methane is divided into indirect conversion, and direct conversion. In indirect conversion, methane is

converted into syngas via reaction, such as steam reforming or partial oxidation; and then other hydrocarbons are produced from the syngas, via the Fischer–Tropsch process or methanol synthesis [6]. Such multi-step process results in high energy consumption. In contrast, by eliminating the intermediate syngas generation step, direct conversion has both energetic and economic advantages [7]. Direct conversion can be classified into oxidative reaction and non-oxidative reaction. Oxidative reaction can increase the reactivity of methane, although most methane is completely oxidized to CO_2 and H_2O [8]. Therefore, non-oxidative reaction is considered a more appropriate approach to increase the selectivity of the desired product. Among the alternative reactions, methane dehydro-aromatization (MDA) is one of the most attractive, because value-added chemicals, such as benzene, toluene, and xylene (BTX), are obtained as products, and can be used as feedstock chemicals in industry [9]. In addition, hydrogen, which is an essential feedstock for chemical industry, is produced with BTX during MDA.

Since Wang et al. first reported the MDA reaction for the production of benzene and hydrogen over Mo oxide supported on HZSM-5 (Mo/HZSM-5) at 700 °C [10], various metals supported on zeolite catalysts have been tested [11]. Previous studies concluded that the most promising catalysts for MDA were Mo supported on zeolites with pore diameters of 5–6 Å, such as ZSM-5, MCM-22, and ZSM-11 [12, 13]. The MDA reaction mechanism on Mo/HZSM-5 was reported to begin with carburization of the supported Mo oxide to Mo oxycarbide or Mo carbide (MoCx) during the reaction [14, 15].

The Mo carbide species activates the C–H bond of methane, which is the rate determining step of MDA [16, 17]. C_2 intermediates derived from the activation of methane are oligomerized, to produce products such as benzene. During the MDA reaction, coke is also formed via additional reaction in the intermediate state, or excessive oligomerization in the product-like state [18]. The formation of coke, unwanted carbonaceous deposit, causes rapid deactivation of the Mo/HZSM-5 catalyst. In particular, the polyaromatic coke formed on the external surface of the zeolite has been regarded as the main deactivation factor among various carbonaceous deposits [19]. Therefore, the major issue in MDA reaction lies in how to increase methane activity, and prevent rapid deactivation arising from coke formation.

In order to improve the methane activity, as well as to inhibit deactivation, various approaches, such as promotor addition and pretreatment, have been undertaken. Although there are conflicting results among the research groups, the performance of the catalyst was enhanced when Fe [20, 21], Co [22, 23], Ni [24], Zn [21], Ga [25, 26], Ag [27], and P [28] were added as promotor. Tan showed that it was possible to increase the benzene yield and stability of Mo/HZSM-5 catalyst by using reaction gas (CH_4) during the pretreatment process [29]. In addition, metallic Ni has also been reported to have excellent methane dissociation ability [30].

Hence, in this study, NiO was selected as a promoter, with anticipation that it could be converted to metallic Ni through the pretreatment process, which was expected to help methane activation. An earlier study

reported that sequentially impregnated Ni-Mo/ZSM-5 increased catalytic activity and stability, because Ni prevents the sublimation of Mo species [31]. For comparison, we prepared Mo/HZSM-5 samples physically mixed with NiO, followed by reductive pretreatment. We found that physically mixed catalysts showed better catalytic performance and stability than the impregnated one. In addition, there is a previous study by Vosmerikov et al. who promoted catalytic activity with Ni addition via physical mixing [24]. However, they used the catalysts prepared by mechanically mixing Mo and Ni nano-sized powders with ZSM-5, not physical mixing of NiO and Mo/HZSM-5 like our study [24]. In this work, the catalytic performance of Mo/HZSM-5 catalyst was enhanced by the use of bulk NiO, which is superior with respect to the simplicity and cost of synthesis procedure. In particular, we further tried to elucidate the role of Ni in enhancing the activity and stability of MDA by investigating the physicochemical properties of the post-reaction samples.

2.2 Experimental

2.2.1. Catalyst preparation

Commercial NH_4-ZSM-5 (Si/Al_2=23, Alfa Aesar) was used as the support of the catalysts. Commercial NH_4-ZSM-5 was calcined in a muffle furnace at 500 °C for 6 h to produce H-ZSM-5. H-ZSM-5 was impregnated with 12 wt.% of Mo by using aqueous solution of ammonium heptamolybdate tetrahydrate (Sigma-Aldrich). The resulting samples were dried at 105 °C overnight, and calcined in a furnace at 500 °C for 6 h. After the calcination, Mo/HZSM-5 and NiO (Sigma-Aldrich) were physically mixed for 10 min using mortar. The physically mixed catalysts are designated XNiO-Mo/HZSM-5(PM), where X is the percentage of the Ni/Mo molar ratio. For example, 10NiO-Mo/HZSM-5(PM) corresponds to 0.73 wt.% of Ni in the sample. To compare with physically mixed catalysts, sequentially impregnated catalysts were also prepared by using aqueous solution of nickel nitrate hexahydrate (Alfa Aesar), following the previous report [31]. The Mo/HZSM-5 was impregnated with the desired Ni/Mo ratio of Ni, and the resulting samples were dried at 105 °C overnight, then calcined in a furnace at 500 °C for 6 h. The impregnated catalysts are designated XNiO-Mo/HZSM-5(IMP), where X is the percentage of the Ni/Mo molar ratio.

2.2.2. Catalytic experiments

The MDA reaction was carried out over 0.2 g of the catalyst in a fixed-bed quartz reactor of 2 cm diameter and 50 cm length. The catalysts were crushed and sieved to 20–40 mesh. Catalyst samples were firstly activated in the reactor as a pretreatment process. The reactor was heated to 400 °C with a ramping rate of 20 °C/min, continuously heated to 700 °C at a ramping rate of 10 °C/min, and maintained for 10 min to stabilize temperature. Pretreatment gas was composed of 45 vol.% CH_4, 5 vol.% He, and 50 vol.% Ar, with a total flow rate of 20 mL/min. When the temperature was stabilized at 700 °C, the MDA reaction started by feeding 90 vol.% CH_4/He gas mixture to the reactor with a flow rate of 10 mL/min at atmospheric pressure. The effluent gases were analyzed at regular intervals by on-line gas chromatograph (YL6500GC) equipped with two columns (GS-Gaspro and Carboxen-1000 columns) and two detectors (flame ionization detector, and thermal conductivity detector). Ar was used as the carrier gas for GC. To prevent condensation and adsorption of the products, such as naphthalene, all the reactor outlet gas lines and gas sampling valves were maintained at 230 °C. Methane conversion and selectivity, and the yield of the carbon-containing products, were evaluated on the basis of carbon mass balance, by using He gas as an internal standard, as reported by Liu et al. [22].

2.2.3. Catalysts characterizations

The crystalline structure of the samples was obtained using powder X-ray diffraction (XRD). XRD was taken on a SmartLab (Rigaku) with Cu Kα radiation at 30 mA and 40 kV. The data was recorded at 2θ range of 5° to 80° with scanning step size of 0.02° at a speed of 2 °/min.

Temperature programmed surface reaction of methane (CH_4–TPSR) was carried out on fresh catalysts to identify the catalyst activation step by using a mass spectrometer (MS, Hiden Analytical). The sample was heated to 100 °C, and maintained for 1 h with 20 mL/min Ar gas to stabilize MS and remove water in the zeolite sample. Next, the gas was switched to 9 mL/min of CH_4, 1 mL/min of He, and 10 mL/min of Ar. The sample was heated to 300 °C at 10 °C/min, and consecutively heated to 900 °C at 2 °C/min. Intensities of H_2, CH_4, CO, Ar, and C_6H_6 were acquired by m/z value of 2, 16, 28, 40, and 78, respectively. Intensity of products was normalized by Ar in the feed.

Pulse CO chemisorption was conducted to compare exposed Mo sites present on the catalysts. Chemisorption measurements were done using BEL-CAT-II coupled with TCD (MicrotracBEL., Corp.) at 50 °C. Samples were pretreated in-situ with H_2 at 700 °C for 40 min since they were exposed to air before loading. A known volume of 4.98 % CO/He passed through a quartz reactor for 1 min. After equilibrium time for 10 min at atmospheric pressure, non-adsorbed CO was detected at the outlet of the reactor. CO pulse repeated until the sample was completely saturated.

Transmission electron microscopy (TEM) and Energy dispersive spectroscopy (EDS) analysis was performed with an accelerating voltage of 200 kV in JEOL-2010 and JEM-ARM200F, respectively. Samples were prepared by dropping the suspension of sample diluted by ethanol on a Lacey-C Cu grid.

Temperature programmed oxidation (TPO) was carried out to examine the nature of carbonaceous deposits of post-reaction samples by using a BEL-CAT BASIC (BEL Japan Inc.) equipped with a MS. Impurities in samples were removed at 300 °C in 50 mL/min of He flow. Post-reaction catalysts (30 mg) were heated from 50 °C to 900 °C with 5 vol.% O_2/He at a heating rate of 5 °C/min. CO_2 (m/z = 44) and CO (m/z = 28) were detected, and all signals were normalized by He.

Visible Raman analysis of the post-reaction catalysts was performed to identify the carbonaceous deposit species present on the catalyst surface. Visible Raman spectra were recorded with a Renishaw (inVia™ Raman Microscope), equipped with CCD detector. The 532 nm line of a Nd:Yag laser was used as the excitation source.

Temperature programmed desorption of NH_3 (NH_3–TPD) was conducted in a BEL-CAT BASIC (BEL Japan Inc.) equipped with a thermal conductivity detector (TCD). Impurities on pretreated samples were removed under He flow at 400 °C for 1 h. Then, samples were exposed to 5 % NH_3/He at 120 °C for 1 h, followed by purging under He flow at 120 °C for 1 h to eliminate weakly adsorbed NH_3 molecules. For NH_3 desorption, samples

were heated to 600 °C under He flow at 10 °C/min.

The numbers of Brønsted and Lewis acid sites were analyzed with Fourier transform infrared (FT-IR) spectrometer (Nicolet 6700, Thermo Fisher Scientific) using pyridine as a probe molecule. The sample was loaded on a wafer and then purged at 400 °C for 2 h under N_2 flow. After collecting the background spectra at 150 °C, pyridine vapor was introduced to the cell at 150 °C. Then, the cell was evacuated at 150 °C for 2 h to remove weakly adsorbed pyridine molecules.

Textural properties of the samples, such as the Brunauer–Emmett–Teller (BET) surface area, t-plot, and Barrett–Joyner–Halenda (BJH) pore size distribution, were obtained by using N_2 physisorption at -196 °C in ASAP 2010 (Micromeritics). The samples were degassed under evacuated condition at 150 °C for 4 h.

2.3. Results and discussions

2.3.1. Methane dehydro-aromatization results

Fig. 2-1 and Fig. 2-2 represent the methane conversion and BTX yield obtained with time-on-stream (TOS) during MDA reaction over Mo/HZSM-5 with NiO-Mo/HZSM-5(IMP) catalysts and NiO-Mo/HZSM-5(PM) catalysts, respectively. Several points should be noted in the catalytic reaction results.

First, the reactivity of the catalysts was compared depending on the Ni loading method. In the case of the impregnation method (Fig. 2-1), 10NiO-Mo/HZSM-5(IMP) showed similar methane conversion to Mo/HZSM-5, while 5NiO-Mo/HZSM-5(IMP) and 20NiO-Mo/HZSM-5(IMP) showed slightly lower methane conversion. BTX yield also did not increase notably, except for 10NiO-Mo/HZSM-5(IMP). In the case of 10NiO-Mo/HZSM-5(IMP), the maximum BTX yield was 5.3 % at 40 min, while the deactivation was much faster than Mo/HZSM-5, resulting in a lower BTX yield after 240 min. Previous study reported that product yield and stability were enhanced by adding Ni via sequential impregnation [31]. However, promoting effect of impregnation was not found in the current study. Such conflict results might be explained by differences in pretreatment condition, Mo loading amount, and reaction condition. On the other hand, in the case of the physically mixed samples (Fig. 2-2), increase in the methane conversion and BTX yield, as well as decrease in the deactivation rate, were clearly observed. In summary, the

sample prepared by the physical mixing method increased the reactivity of the catalyst much more significantly than those by the impregnation method.

Secondly, the effects of the contents of NiO on the reactivity of NiO-Mo/HZSM-5(PM) samples were compared. The addition of NiO below the Ni/Mo ratio of 20 % contributed to the increase of the methane conversion and BTX yield. In the case of Mo/HZSM-5, the initial conversion was 12.0 %, and the conversion at 840 min was 5.7 %, with the maximum BTX yield of 4.7 % at 80 min. On the other hand, in the case of 10NiO-Mo/HZSM-5(PM), the maximum initial conversion was 13.0 %, and the conversion at 840 min was 8.5 %, with the maximum BTX yield of 5.6 % at 340 min. Furthermore, the BTX yield of 10NiO-Mo/HZSM-5(PM) was about two times higher than that of Mo/HZSM-5 at 840 min, indicating the enhanced stability. The optimal Ni/Mo ratio was 10 %, in terms of the maximum conversion and BTX yield. The higher methane conversion and BTX yield of NiO-Mo/HZSM-5(PM) than Mo/HZSM-5 indicate that the physically mixed NiO plays a crucial role in enhancing the methane activation ability, and maintaining the activity during reaction.

However, when the Ni/Mo ratio was higher than 50 %, the reaction trend was completely changed. In addition, when the Ni/Mo ratio increased from 50 % to 100 %, the initial methane conversion significantly increased from 15 % to 20 %, followed by an abrupt decrease. Although the initial methane conversion was high on the catalyst, it can be interpreted that NiO-related species itself converted methane to coke quite actively, rather than to

BTX, based on the fact that BTX was not produced in the reaction. This result implies that when excessive NiO is physically mixed with Mo/HZSM-5, NiO-related species not only helps MDA reaction via methane activation, but also consumes methane as coke on their own.

The catalytic reaction results of NiO/HZSM-5(PM), which was prepared by the physical mixing of NiO and HZSM-5, are shown in Fig. 2-3. The content of NiO in NiO/HZSM-5(PM) was equal to that in 50NiO-Mo/HZSM-5(PM). NiO/HZSM-5(PM) showed high methane conversion at the beginning of the reaction, and then drastically declined to 3 %. Also, despite the presence of Brønsted acid site (BAS) on the HZSM-5, no product was detected, even though methane was converted. This implies that NiO-related species was able to activate methane to convert to coke, without producing aromatic compounds. To sum up, NiO was actively involved in enhancing both methane activation, and coke formation.

Fig. 2-2(b) shows that the induction period becomes longer as the loading amount of NiO increases. The induction period is defined as when the methane conversion is high, although BTX is not produced during the initial reaction stage. It is known that during the induction period, molybdenum carbide-like species, which are well known as active sites of methane activation, are formed to generate hydrocarbon pools, a precursor to BTX [13, 32]. This result implies that the addition of NiO is able to affect the reaction pathway of Mo/HZSM-5, especially when NiO was introduced by a physical mixing method, rather than by an impregnation method.

We obtained the deactivation rate during the MDA reaction, which was calculated by applying linear fitting to the BTX yield. The range of TOS was determined as the time difference between the BTX yield reaching its maximum, and 840 min. Table 2-1 shows that the deactivation rate decreased with increasing NiO contents. In other words, increasing the amount of NiO enhanced stability in the MDA reaction. Samples with Ni/Mo ratio of above 50 % were ignored, due to the abnormal trend of reaction that was not deactivated by 840 min. However, because deactivation absence also means stability enhancement, we can claim that the stability of the catalysts increases with the increase of NiO addition.

Fig. 2-4 represents the overall product distribution and the total amount of converted methane for Mo/HZSM-5 and NiO-Mo/HZSM-5(PM). The overall product distribution and the total amount of converted methane is calculated by integrating 14-hour reaction data. Product selectivity showed that the main product was benzene, followed by naphthalene and toluene. The selectivity of toluene and xylene was so small, at less than 0.1 and 0.01 times that of benzene, respectively, that it was reasonable to analyze benzene mainly. In addition, the addition of NiO with a Ni/Mo ratio over 20% resulted in increase of the overall coke selectivity with the increase of the total amount of converted methane. Increased coke selectivity can be explained by coke formation by NiO species. However, when NiO was added with a Ni/Mo ratio below 20%, the overall coke selectivity was decreased even with the increase in the total amount of converted methane. This result represents that the

addition of optimum amount of NiO enhances the catalytic activity by preventing methane from being converted to coke. Moreover, the highest benzene selectivity of 10NiO-Mo/HZSM-5(PM) and lower naphthalene selectivity compared to Mo/HZSM-5 catalysts supports this explanation. It is known that naphthalene tends to polymerize into heavier polyaromatic species; in other words, a precursor to coke [33]. Such behavior suggests that the lower selectivity of naphthalene on 10NiO-Mo/HZSM-5(PM) implies the formation of less carbonaceous deposits in the zeolite, which causes deactivation [34]. Thus, the formed carbonaceous deposits are expected to block the active site and pores, which lead to the deactivation as the reaction proceeds. In other words, the improved stability of NiO-Mo/HZSM-5(PM) catalyst is closely related to decreased naphthalene selectivity, resulting from NiO addition.

Hydrogen (H_2) is another essential chemical compound obtained during MDA. Therefore, it is important to obtain the amount of produced H_2. Fig. 2-5 represents the sum of H_2 production of catalysts during 14 h of reaction, which was calculated from reaction results. When Ni content in the catalyst increased, H_2 production increased. While Mo/HZSM-5 produced 116.3 mmol/gcat of H_2, 100NiO-Mo/HZSM-5(PM) yielded 330.9 mmol/gcat. Although 20NiO-Mo/HZSM-5(PM), 50NiO-Mo/HZSM-5(PM) and 100NiO-Mo/HZSM-5(PM) had less BTX yield than 10NiO-Mo/HZSM-5(PM), H_2 formation rate was higher. Therefore, it can be inferred that increased H_2 production over 20NiO-Mo/HZSM-5(PM) to 100NiO-Mo/HZSM-5(PM)

arises from increased coke formation, not increased product formation.

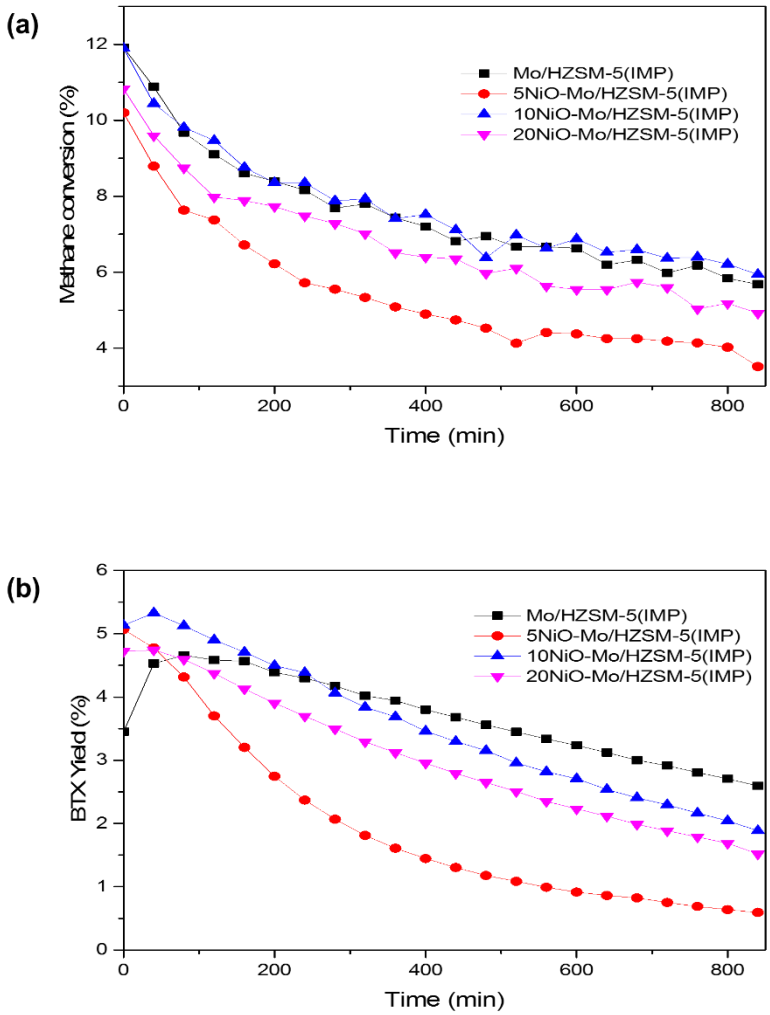

Fig. 2- 1. Catalytic performance of NiO-Mo/HZSM-5(IMP) catalysts with various Ni/Mo ratios: (a) Methane conversion, and (b) BTX yield.

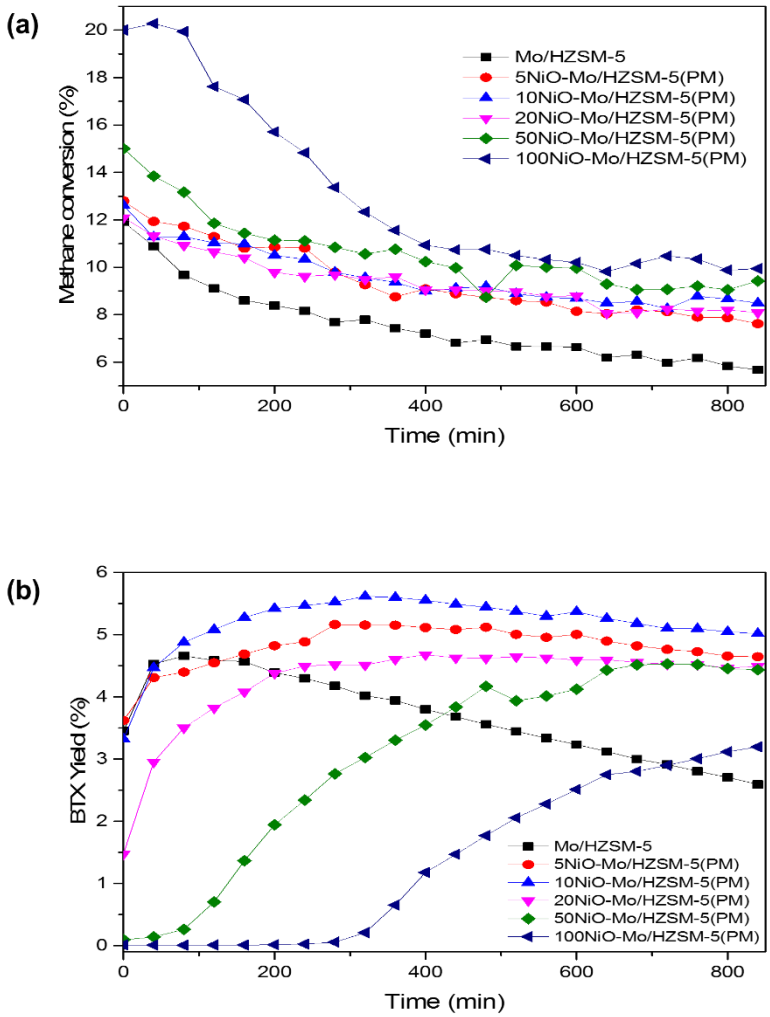

Fig. 2- 2. Catalytic performance of NiO-Mo/HZSM-5(PM) catalysts with various Ni/Mo ratios: (a) Methane conversion, and (b) BTX yield.

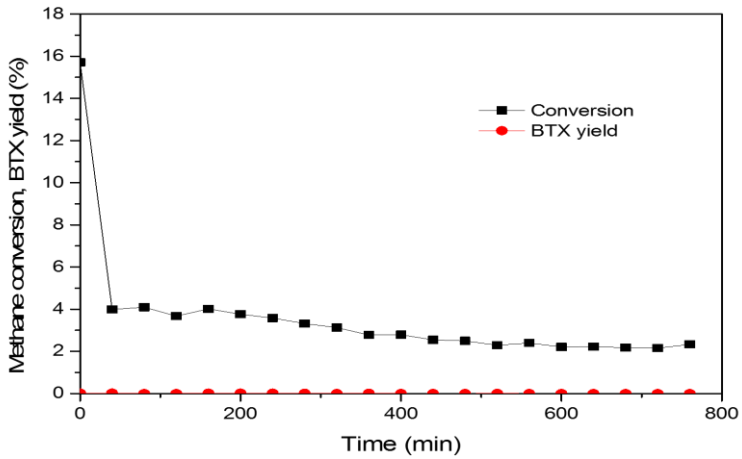

Fig. 2- 3. Methane conversion and BTX yield of NiO/HZSM-5(PM) catalyst.

Catalyst	Deactivation rate (10^{-3}/min)	R^2
Mo/HZSM-5	2.85	0.998
5NiO-Mo/HZSM-5(PM)	1.22	0.937
10NiO-Mo/HZSM-5(PM)	1.02	0.977
20NiO-Mo/HZSM-5(PM)	0.44	0.896

Table 2- 1. Deactivation rate of catalysts.

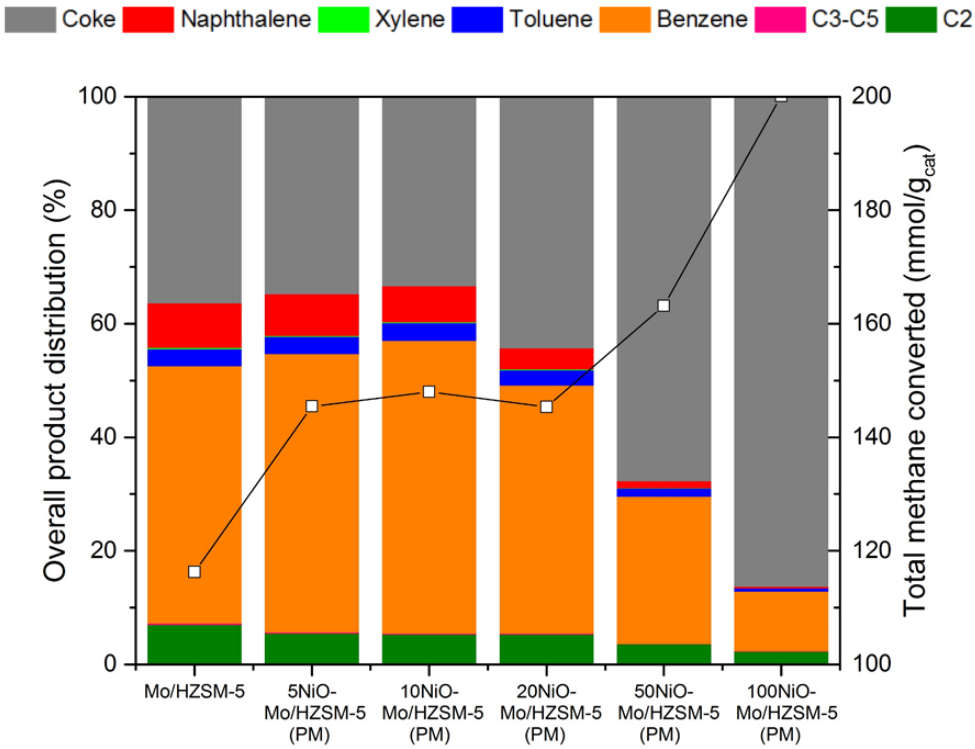

Fig. 2- 4. Overall product distribution and total amounts of converted methane of the NiO-Mo/HZSM-5(PM) catalysts with various Ni/Mo ratio.

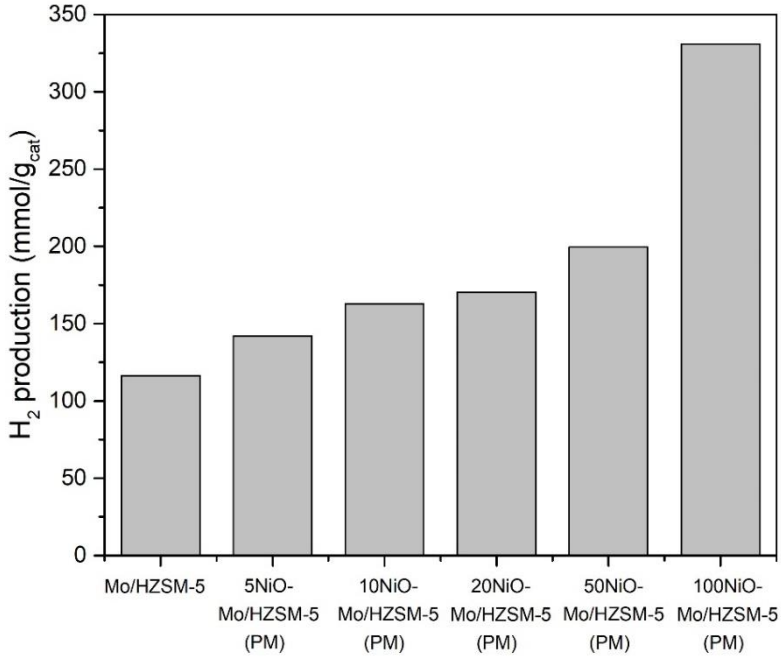

Fig. 2- 5. The amount of cumulative H_2 production over NiO-Mo/HZSM-5(PM) catalysts with various Ni/Mo ratios during 14 h of reaction.

2.3.2. Role of NiO in the catalyst activation step

2.3.2.1. Phase transition in the catalyst activation step

Fig. 2-6 (a) and (b) show the XRD patterns of fresh and pretreated catalysts. The XRD patterns of all samples match well with their zeolite supports, HZSM-5. However, the peak intensity of ZSM-5 in Mo-impregnated catalysts is slightly lower than that of the pure HZSM-5, which is probably attributed to the migration of molybdenum oxide into the zeolite channels [35]. In addition, average crystallite size of bulk NiO was 38 nm, which was calculated by the Scherrer equation (Fig. 2-7).

In the case of fresh catalysts, the peak at 2θ of 27.3° assigned to MoO_3 phase was detected. This means that even after the calcination, not all molybdenum oxide could be highly dispersed on the zeolite surface. Fresh NiO-Mo/HZSM-5(PM) samples demonstrated the peaks arising from NiO phase, although no mixed phase peaks of Mo–Ni were observed.

Fig. 2-6(b) shows the XRD patterns of the pretreated catalysts. No peaks arising from Mo-related phase were observed in all pretreated catalysts. These results indicate that during the pretreatment process, crystalline MoO_3 located on the external surface of zeolite became highly dispersed and carburized. In addition, the appearance of peaks corresponding to metallic Ni in the pretreated NiO-Mo/HZSM-5(PM) implies that during the pretreatment process, NiO was reduced to metallic Ni. Also, note that no peak arising from the Mo and Ni mixed crystalline phases was detected over pretreated NiO-Mo/HZSM-5(PM). Therefore, evolution of active species was clarified by

CH_4–TPSR, CO chemisorption and TEM in the next section.

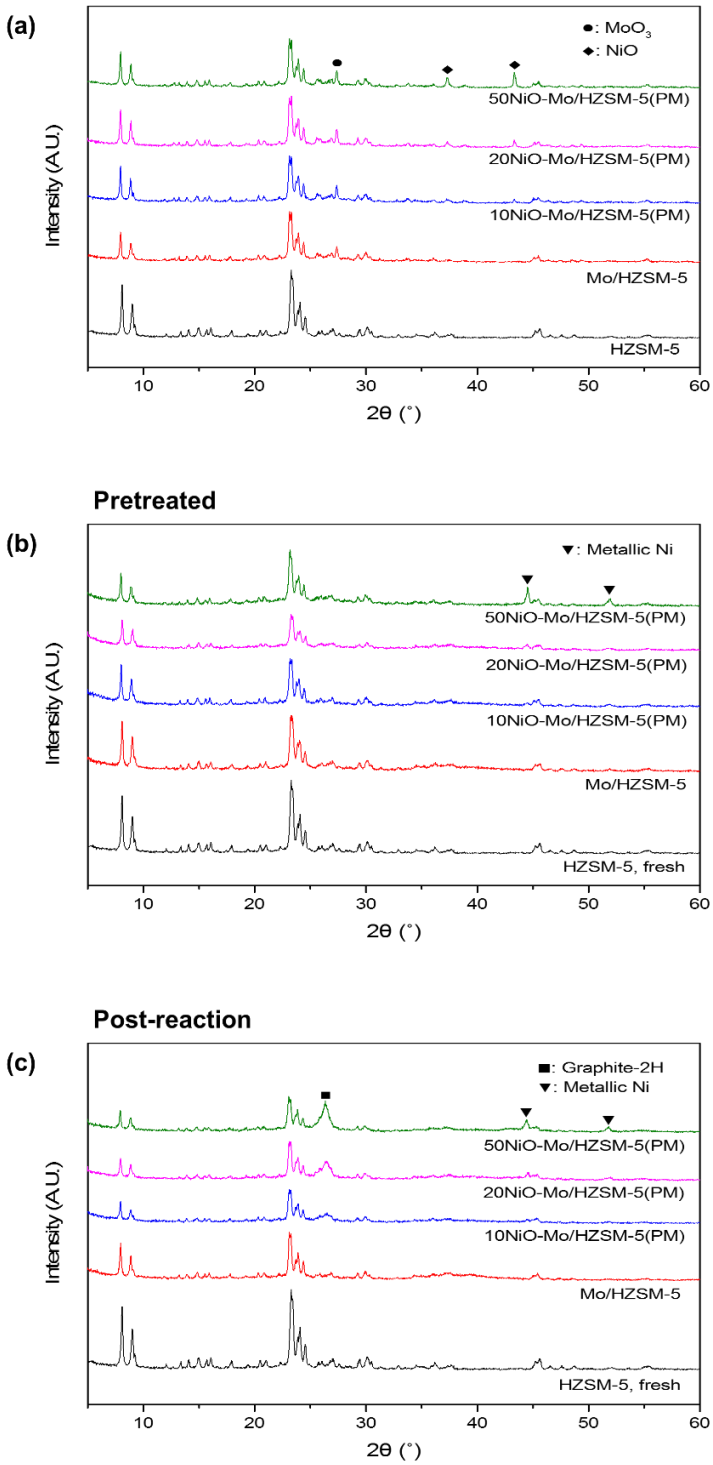

Fig. 2- 6. The XRD patterns for (a) fresh catalysts, (b) pretreated catalysts, and (c) post-reaction catalysts (after reaction for 840 min).

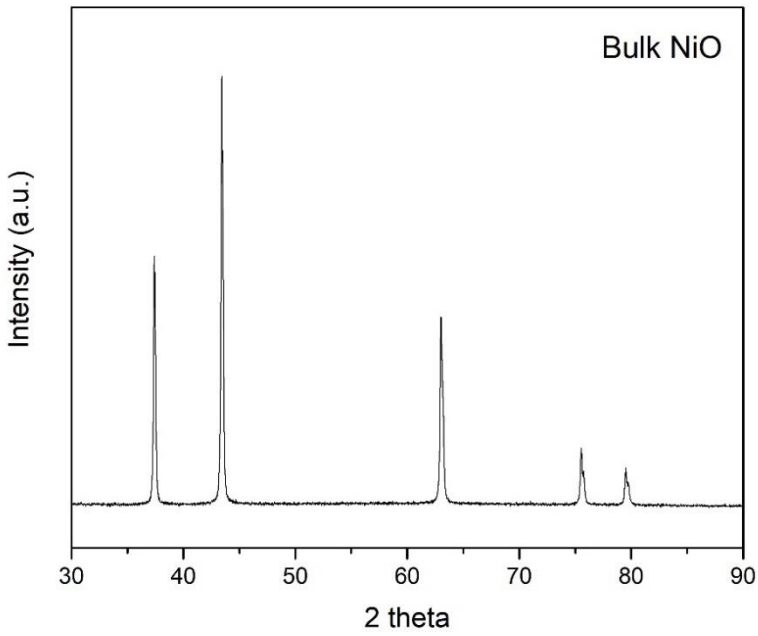

Fig. 2- 7. The XRD pattern for bulk NiO.

2.3.2.2. Monitoring the evolution of active species with CH_4-TPSR

Fig. 2-8 presents the CH_4–TPSR results of catalysts. During the pretreatment step, NiO and MoOx are reduced to metallic Ni and MoCx, respectively, as confirmed by XRD. The reduction sequence of these two oxides is expected to be clarified through CH_4–TPSR. Furthermore, the activation scheme of NiO-Mo/HZSM-5(PM) catalysts during the MDA reaction can be understood by analyzing temperature where various products, such as H_2O, CO, and C_6H_6, begin to form.

First, Fig. 2-8(a) shows that Mo/HZSM-5 presented a H_2 peak and a CO peak at 675 °C, which originated from the reduction of MoOx to MoCx by CH_4. The evolution of benzene began to appear at 685 °C, verifying that MoCx is an active phase of benzene formation, which is consistent with the previous literature [36, 37]. Fig. 2-8(b) shows that bulk NiO was reduced to simultaneously produce H_2 and CO to form metallic Ni state at 576 °C. In addition, as the temperature reaches 657 °C, H_2 production increases again, because the metallic Ni transforms methane into coke and H_2. Note that although CH_4 was consumed, benzene was not produced over bulk NiO, which is consistent with the activity result of NiO/HZSM-5(PM) in Fig. 2-3.

In the case of NiO-Mo/HZSM-5(PM) (Fig. 2-8(c)–(e)), all NiO-Mo/HZSM-5(PM) catalysts showed two peaks of H_2 and CO evolution. Based on the CH_4–TPSR results over bulk NiO and Mo/HZSM-5, it can be claimed that the first evolution peaks of H_2 and CO at 574 °C–578 °C are attributed to CH_4 decomposition during the reduction of NiO to metallic Ni,

while the peaks at high temperature above 630 °C are due to the reduction of MoOx to MoCx. In particular, the peak shift of MoOx reduction temperature can be recognized as a function of the Ni/Mo ratio of the NiO-Mo/HZSM-5(PM) catalysts. In the case of 10NiO-Mo/HZSM-5(PM) and 20NiO-Mo/HZSM-5(PM), the second H_2 and CO peaks arising from the reduction of MoOx were located at around 633 °C. This indicates that the reduction temperature of MoOx in 10NiO-Mo/HZSM-5(PM) was lower than in Mo/HZSM-5 by 40 °C. In addition, the benzene formation temperature decreased from 685 °C to 649 °C and 647 °C for 10NiO-Mo/HZSM-5(PM) and 20NiO-Mo/HZSM-5(PM), respectively. It was reported that migration of MoOx can occur above its Tammann temperature (534 K) because lattice mobility within MoO_3 becomes possible [38]. The CH_4–TPSR results clearly showed that MoCx was formed at relatively high temperature of 675 °C over Mo/HZSM-5, allowing MoOx to agglomerate with higher mobility and block zeolite pores before being reduced, thus forming a less dispersed MoCx. On the other hand, in case of 10NiO-Mo/HZSM-5, metallic Ni helped MoOx to reduce at 633 °C, which was 40 °C lower than MoOx reduction temperature of Mo/HZSM-5. Lower reduction temperature allowed MoOx to have less mobility, resulting in higher dispersion of MoCx. These results confirm that metallic Ni facilitates the reduction of MoOx, as well as the formation of MoCx, resulting in the promotion of benzene production. To sum up, these results suggest that methane reacts with NiO during the pretreatment step to form metallic Ni, and metallic Ni helps MoOx to be converted to MoCx with

higher dispersion at lower temperature. To clarify this point, MoCx dispersion was further analyzed by CO chemisorption and TEM in the next section.

However, 50NiO-Mo/HZSM-5(PM) (Fig. 2-8(e)) showed a broad H_2 peak at 581 °C–668 °C, which was caused by intensive coke formation. Because of this broad H_2 peak, the peak of MoOx reduction could not be clearly identified. Such intensive coke formation implies that excessive metallic Ni could convert CH_4 to coke. Benzene formation over 50NiO-Mo/HZSM-5(PM) was initiated at 670 °C, which was lower than over Mo/HZSM-5 by 15 °C, but higher than over 10NiO-Mo/HZSM-5(PM) and 20NiO-Mo/HZSM-5(PM) by approximately 20 °C. Such a shift can explain the longer induction period of 50NiO-Mo/HZSM-5(PM) during the MDA reaction. The induction period includes not only MoCx formation time, but also the time for developing hydrocarbon pool. To produce aromatic hydrocarbons, aromatic intermediates need to be concentrated inside the zeolite pore, and stabilized by secondary reactions, which is termed the hydrocarbon pool mechanism [9, 39]. For the case of 50NiO-Mo/HZSM-5(PM), the reactions between CH_4 and metallic Ni were dominant, which would have led to deficient hydrocarbon pool formation. It is highly probable that if an excessive amount of NiO was used, benzene formation would be suppressed at an initial stage, because hydrocarbon pool formation would be delayed, as shown in the activity results in Fig. 2-2.

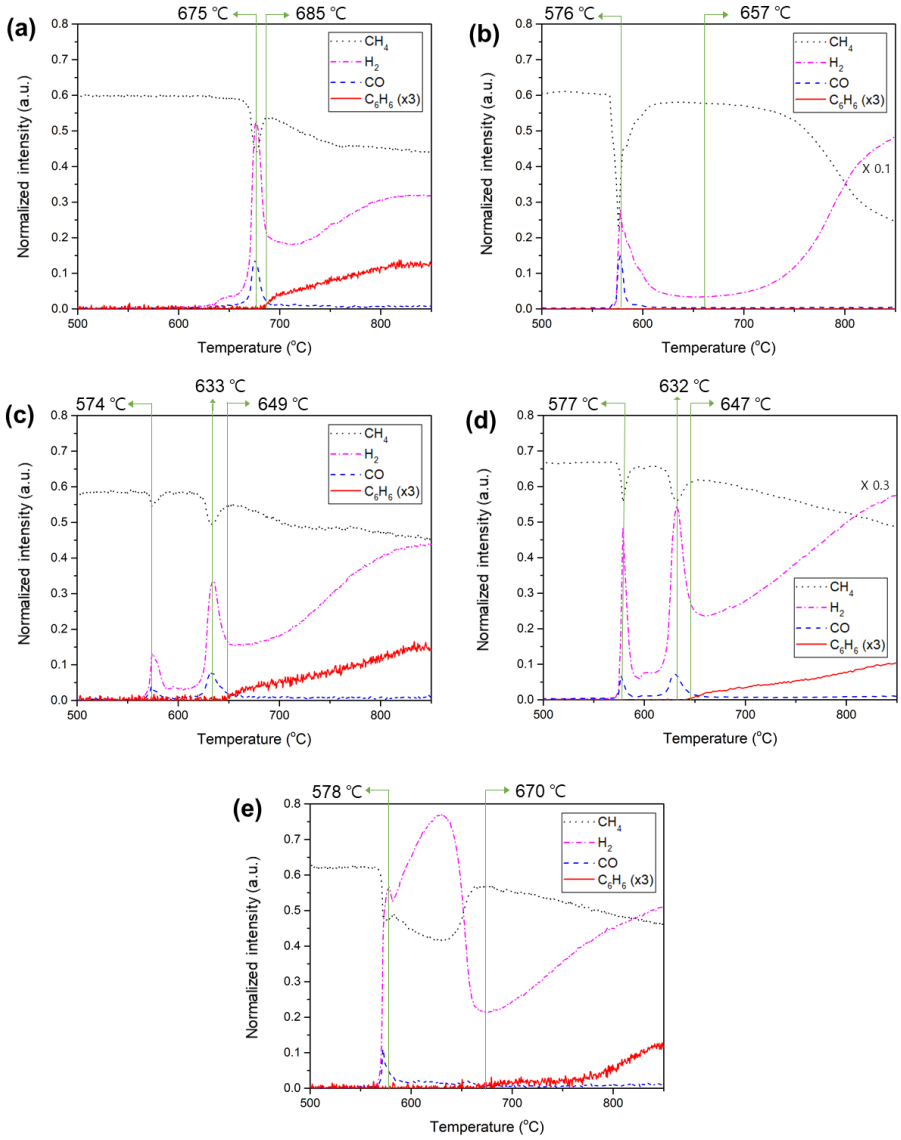

Fig. 2- 8. CH_4–TPSR profiles of (a) Mo/HZSM-5, (b) the bulk NiO, (c) 10NiO-Mo/HZSM-5(PM), (d) 20NiO-Mo/HZSM-5(PM), and (e) 50NiO-Mo/HZSM-5(PM).

2.3.2.3. Analysis of MoCx dispersion with CO chemisorption and TEM

MoCx dispersion of pretreated and post-reaction catalysts were compared based on CO chemisorption and TEM analyses (Table 2-2). CO uptake by MoCx was calculated by subtracting CO uptake by the support and Ni to exclude chemisorption on the support and the promoter (Table 2-3). Post reaction samples had less CO uptake than pretreated samples, which means that CO chemisorbed on coke were negligible. After the addition of NiO by physical mixing, CO uptake of the pretreated catalysts increased from 0.19 cm^3g^{-1} to 0.64 cm^3g^{-1}. In the case of post-reaction catalysts, CO uptake increased from 0.08 cm^3g^{-1} to 0.55 cm^3g^{-1} after NiO addition. Hence, it is confirmed that 10NiO-Mo/HZSM-5(PM) had more CO uptake than Mo/HZSM-5 on both pretreated and post-reaction samples, thus providing a convincing evidence about higher MoCx dispersion.

Mean diameter of Mo particles which were calculated from TEM was in line with CO chemisorption results. Fig. 2-9(a)–(d) presents the TEM images and corresponding size distribution diagrams of Mo/HZSM-5 and 10NiO-Mo/HZSM-5(PM), in order to compare the size of MoCx and coke particles in the samples. Based on the TEM result, only the size of MoCx and carbon except Ni was measured. Since the morphology of the particle was irregular, particle diameter was defined as the diameter of a circle that had the same area as the measured particle area. Mean diameter of MoCx and the coke particles of the pretreated catalysts was reduced from 10.2 nm to 6.6 nm after the addition of NiO. Moreover, for the case of post-reaction catalysts,

after NiO addition, the diameter was reduced from 14.0 nm to 8.2 nm. This indicates that when NiO was added, the growth of MoCx particles and coke formed on Mo sites and zeolite was significantly suppressed. Higher activity of 10NiO-Mo/HZSM-5(PM) could be explained by higher dispersion of MoCx, as can be seen from CO chemisorption and TEM.

	Catalysts	CO uptake (cm^3g^{-1})[a]	d_{va} (nm)[b]
Pretreated	Mo/HZSM-5	0.19	10.2
	10NiO-Mo/HZSM-5(PM)	0.64	6.6
Post-reaction	Mo/HZSM-5	0.08	14.0
	10NiO-Mo/HZSM-5(PM)	0.55	8.2

[a] Calculated from pulse CO chemisorption (Chemisorption stoichiometry: 1)
[b] Calculated by TEM

Table 2- 2. CO uptake and mean diameter of Mo particles over pretreated and post-reaction catalysts.

Sample	CO uptake (cm^3g^{-1})[a]
HZSM-5	0.15
NiO(1.06 wt.%)/HZSM-5(PM)[a]	0.18
Pretreated Mo/HZSM-5 [b]	0.33
Pretreated 10NiO-Mo/HZSM-5(PM) [c]	0.80
Post-reaction Mo/HZSM-5 [b]	0.21
Post-reaction 10NiO-Mo/HZSM-5(PM) [c]	0.70

[a] 1.06 wt.% NiO is equivalent to amount of NiO in 10NiO-Mo/HZSM-5(PM)
[b] Before subtracting CO chemisorption on HZSM-5
[c] Before subtracting CO chemisorption on NiO(1.06 wt.%)/HZSM-5(PM)
*Excluded adsorption on support (HZSM-5, NiO(1.06 wt.%)/HZSM-5(PM))
Vm (Mo) = Vm (total) - Vm (support)
Vm (support) = m (support) * V (sole support) / m (sole support)
m (support) = m (total) * (1-C(wt. proportion)) * (1-Mo(wt. proportion))

Table 2- 3. CO uptake and mean diameter of Mo particles over pretreated and post-reaction catalysts.

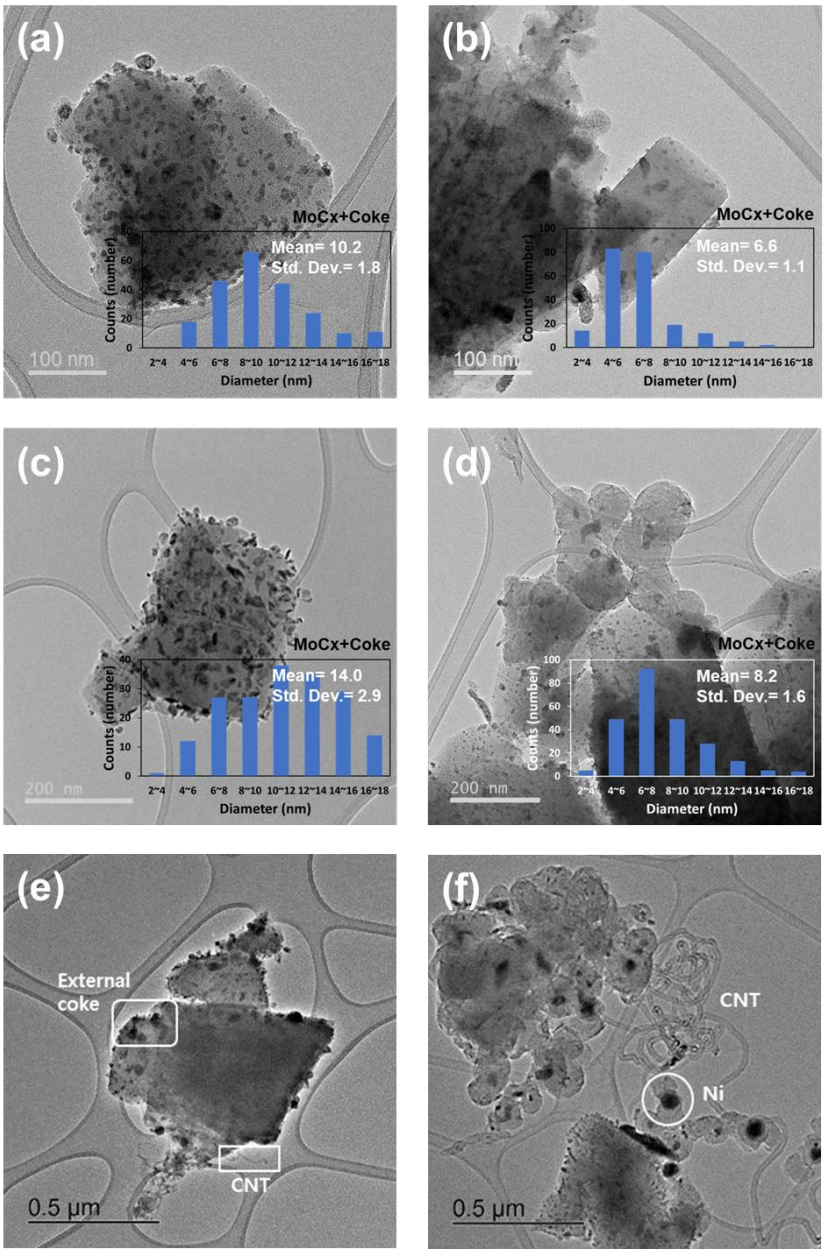

Fig. 2- 9. TEM images with diameter distribution diagram of MoCx and coke for (a) pretreated Mo/HZSM-5, (b) pretreated 10NiO-Mo/HZSM-5(PM), (c) post-reaction Mo/HZSM-5, and (d) post-reaction 10NiO-Mo/HZSM-5(PM). TEM images of post-reaction (e) Mo/HZSM-5, and (f) 10NiO-Mo/HZSM-5(PM).

2.3.2.4. Acid distribution analysis using NH_3–TPD and pyridine FT–IR for examination of MoCx dispersion

It was reported that active MoCx nanoparticles prefer to anchor on framework Al site, referred as Brønsted acid site (BAS) [40]. Therefore, dispersion of MoCx could be inferred by measuring the number of BAS. If anchored MoCx inside zeolite pore increases, more anchoring site on framework Al would have been occupied, resulting in the reduced number of BAS.

In order to determine the number of BAS content in the catalysts, NH_3–TPD and pyridine FT–IR were performed. NH_3–TPD result (Fig. 2-10) shows total acidity of pretreated catalysts. It can be seen that total acidity decreased over pretreated 10NiO-Mo/HZSM-5(PM). Since MoCx has negligible acid sites [41], the number of acid sites is obtained by integrating the amount of desorbed NH_3 species from hydrogen-bonded physisorption sites, Lewis acid site (LAS) and Brønsted acid site (BAS) [42]. In addition, acid distribution of the catalysts can be clarified by using IR spectra of pyridine adsorption (Fig. 2-11). The band at 1547 cm^{-1} is attributed to BAS, and the band at 1455 cm^{-1} is to LAS [43].

Quantitative analysis of acid distribution of pretreated catalysts are summarized in Table 2-4. The number of BAS and LAS were obtained by measuring the amount of NH_3 desorbed above 300 °C during NH_3–TPD [44]. Proportion of acid sites were acquired from pyridine FT–IR by calculating peak area of adsorbed pyridine using extinction coefficients, 1.67 cm/μmol

for BAS and 2.22 cm/μmol for LAS [43]. Concentration of BAS decreased from 226 μmol/g to 118 μmol/g after the addition of NiO. Also, [B]/[L] ratio was significantly lowered over 10NiO-Mo/HZSM-5(PM), indicating that higher amount of BAS was occupied with MoCx upon the addition of NiO. This result clearly indicates that NiO addition facilitated anchoring of MoCx on framework Al, enhancing dispersion inside zeolite channels.

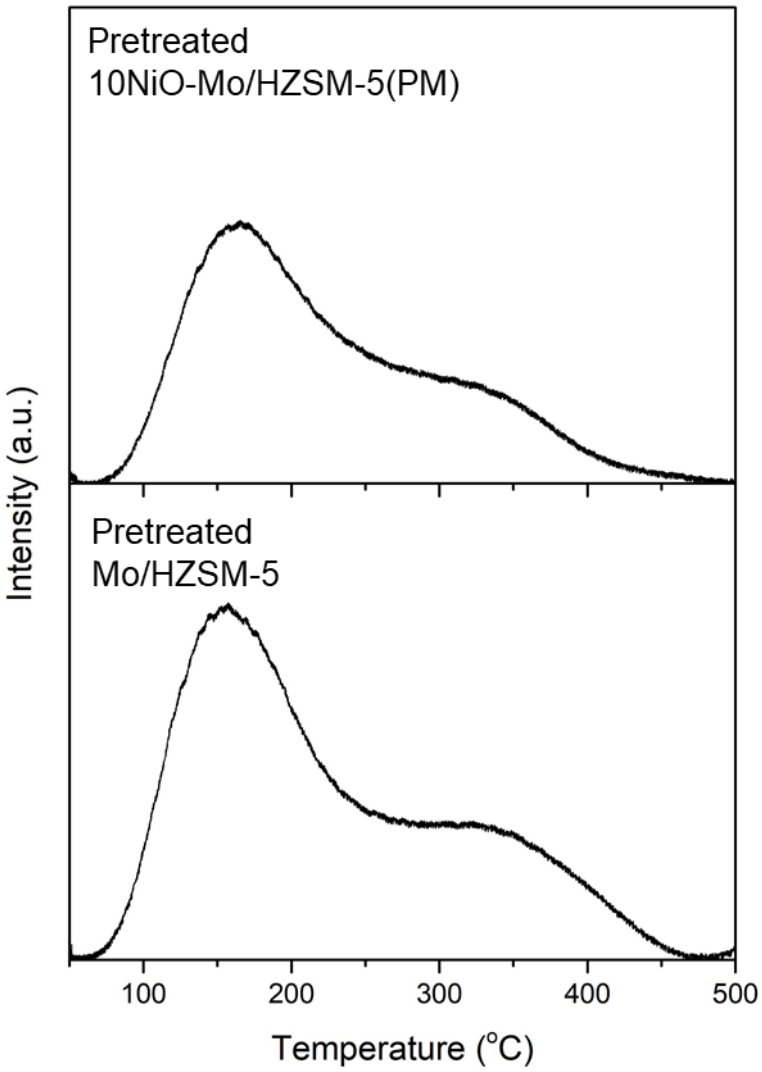

Fig. 2- 10. NH_3-TPD profiles of pretreated catalysts.

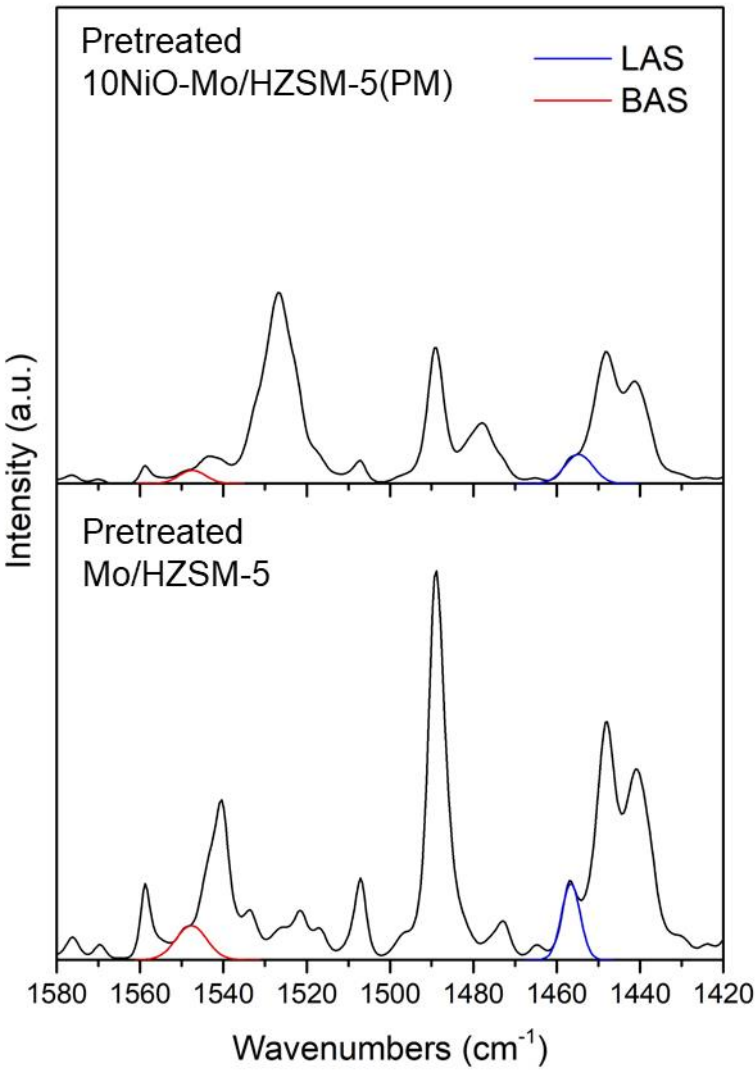

Fig. 2- 11. FT-IR spectra for pyridine adsorption on pretreated catalysts.

Catalysts	Brønsted acid site (μmol/g)	Lewis acid site (μmol/g)	Brønsted/Lewis acid site ratio ([B]/[L])
Pretreated Mo/HZSM-5	226	229	0.98
Pretreated 10NiO- Mo/HZSM-5(PM)	118	208	0.57

Table 2- 4. Acid distribution of pretreated catalysts.

2.3.3. Effect of NiO on the catalyst deactivation

2.3.3.1. Phase transition of post-reaction catalysts

Fig. 2-6(c) shows the XRD patterns of post-reaction (after 840min reaction) catalysts. Even after reaction, their zeolite support structures were maintained. The XRD patterns of post-reaction NiO-Mo/HZSM-5(PM) samples exhibited metallic Ni peaks at 44.5° and 51.7°, and a graphite-2H peak at 26.4°, which were totally different from those of the post-reaction Mo/HZSM-5. As the loading of NiO increased, the intensity of these two peaks increased. Also, no peak corresponding to mixed Mo–Ni phases was observed in all the XRD patterns of the post-reaction NiO-Mo/HZSM-5(PM) catalysts. These results indicate that metallic Ni initially formed by the pretreatment process was maintained during the reaction. Furthermore, it presents that graphite-2H peak related carbonaceous deposits are formed, resulting from the physical mixing with NiO. It is reported that Graphite-2H peak originates from carbon nanotube (CNT) [45], which are further analyzed by using TEM and visible Raman described in the next section.

2.3.3.2. Investigation of coke species with TEM, TPO and visible Raman spectroscopy

The morphology of the post-reaction catalysts analyzed by TEM is displayed in Fig. 2-9(e)–(f) and Fig. 2-12. First, large coke particle on the external surface was observed in the Mo/HZSM-5 sample. It was reported that external acid sites play a major role in depositing coke [19]. Also, a small amount of carbon nanotube (CNT) could be seen on the post-reaction Mo/HZSM-5, as shown in Fig. 2-9(e). However, it is interesting to note that a large amount of CNT was observed on the post-reaction NiO-Mo/HZSM-5(PM) samples in Fig. 2-9(f) and Fig. 2-12. As the NiO content increased, the amount of CNT dramatically increased. It is well known that metallic Ni is the catalyst for CNT production [46]. Also, the EDS images in Fig. 2-13 show that carbon was mainly deposited on Ni rather than on zeolite, supporting that Ni is active site for producing CNT. It should be noted that the deposition of CNT and graphite-like coke was concentrated in the vicinity of Ni particle, since the EDS mapping result indicates that the C- and Ni-rich regions are mostly overlapped.

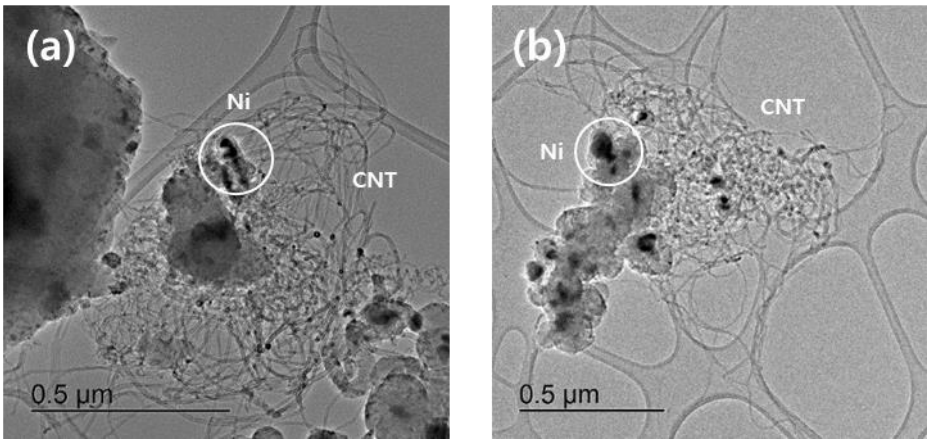

Fig. 2- 12. TEM images of post-reaction (a) 20NiO-Mo/HZSM-5(PM) and (b) 50NiO-Mo/HZSM-5(PM).

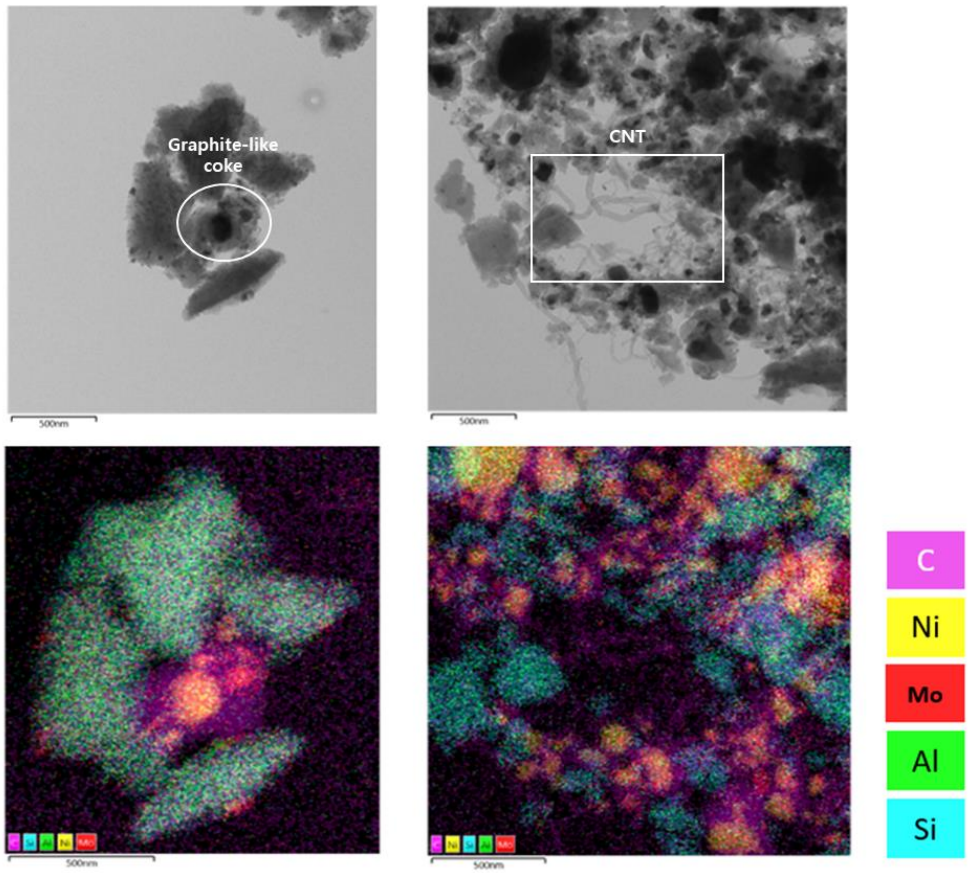

Fig. 2- 13. TEM images and corresponding EDS mapping analysis data of C, Ni, Mo, Al and Si for post-reaction 50NiO-Mo/HZSM-5(PM).

TPO was used to investigate the characteristics of coke in post-reaction catalysts (Fig. 2-14). Coke species were classified into low-temperature coke (LT coke) and high-temperature coke (HT coke), depending on the temperature where CO_2 was evolved. LT coke, which was assigned to a peak at 400 °C–600 °C, was generated in all catalysts. Therefore, it is reasonable to suppose that LT coke contains coke from Mo/HZSM-5, which is consistent with previous studies [47, 48]. Coke generated in Mo/HZSM-5 contains graphite-like coke or aromatic coke, which is formed predominantly on external MoCx and external Brønsted acid site on zeolite [19, 47]. Table 2-5 shows the amount of LT coke, which in all catalysts did not vary considerably, implying that the amount of coke on MoCx and Brønsted acid site did not significantly increase, resulting from the physical mixing with NiO.

On the other hand, as the NiO content increased, a new type of coke (HT coke), which was located over 600 °C, increased remarkably. This suggests that NiO induces the formation of HT coke. As observed in previous TEM results, carbon nanotube was produced more abundantly on Ni particles. Therefore, it can be inferred that HT coke is related to the carbon nanotube produced on Ni. Xu et al. also reported that TPO peak above 600 °C was attributed to CNT, which was produced from Fe during the MDA reaction [48]. It appears that increased coke formation over NiO-Mo/HZSM-5(PM) can be attributed to carbon nanotube on Ni, rather than coke on MoCx and zeolite.

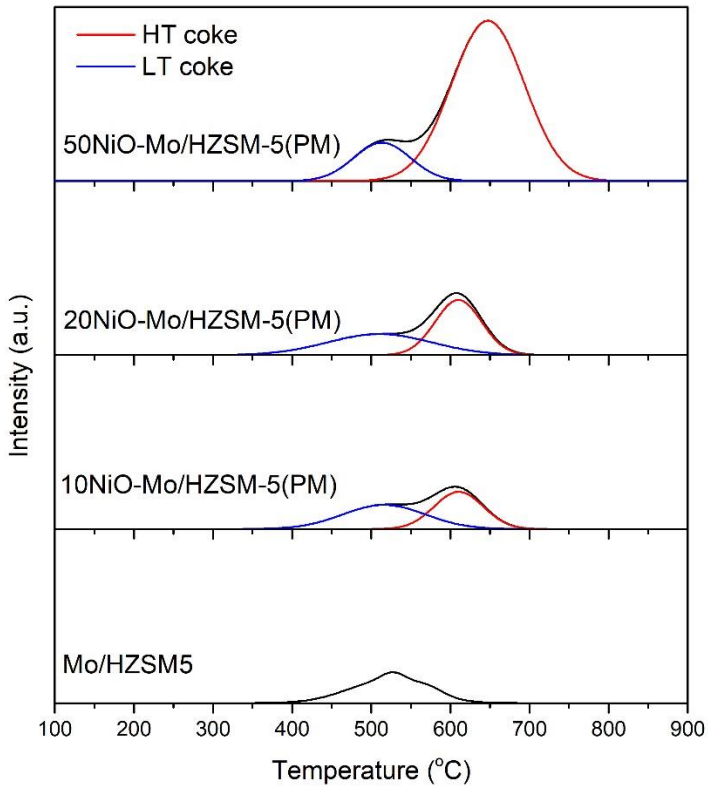

Fig. 2- 14. TPO profiles of the post-reaction catalysts.

Area	Mo/HZSM-5	10NiO-Mo/HZSM-5(PM)	20NiO-Mo/HZSM-5(PM)	50NiO-Mo/HZSM-5(PM)
LT coke	0.77	0.73	0.79	0.79
HT coke	-	0.67	0.93	4.26

Table 2- 5. TPO peak area of the post-reaction catalysts.

Visible Raman analysis was performed to examine the coke species more precisely. Fig. 2-15 displays the Raman spectra of graphite, CNT, and the post-reaction catalysts. Both graphite and CNT had D, G, and 2D peaks at similar locations to the previous studies [49]. CNT had an asymmetric G peak and higher D/G ratio than graphite, due to the curved structure [50]. The largest difference between graphite and CNT lies in the position of the 2D peak. Graphite had an asymmetric 2D peak at 2,715 cm^{-1}, whereas CNT had a symmetric 2D peak at 2,689 cm^{-1}, which results are in good agreement with the previous studies [49-51].

All NiO-Mo/HZSM-5(PM) post reaction samples had almost identical Raman spectra. They had D (1,338 cm^{-1}), asymmetric G (1,570 cm^{-1}), and symmetric 2D (2,676 cm^{-1}) peaks, which were similar to the features of CNT. This implies that CNT is the dominant coke species over NiO-Mo/HZSM-5(PM), consistent with the TEM and TPO results. However, Mo/HZSM-5 had distinctive features of Raman spectra, such as broad D peak of 1,000 cm^{-1}–1,490 cm^{-1}, shifted G peak of 1,605 cm^{-1}, and absence of the 2D peak. Such changes in Raman spectra are probably attributed to the presence of disordered sp^3 carbon in the post-reaction Mo/HZSM-5 [49, 52, 53]. It was reported that as the sp^3/sp^2 fraction increases, the carbon becomes more amorphous, resulting in alteration of the Raman spectra [53]. Previous study also revealed the presence of both amorphous and graphitic coke on post-reaction Mo/HZSM-5 sample, which is in good agreement with the current study [34]. Amorphous coke is known as the coke generated on MoCx,

which accelerates catalyst deactivation [54]. Therefore, it is reasonable to suppose that Mo/HZSM-5 is vulnerable to coke on MoCx, while the addition of NiO prevents coke formation on MoCx by producing CNT on Ni, extending catalytic stability.

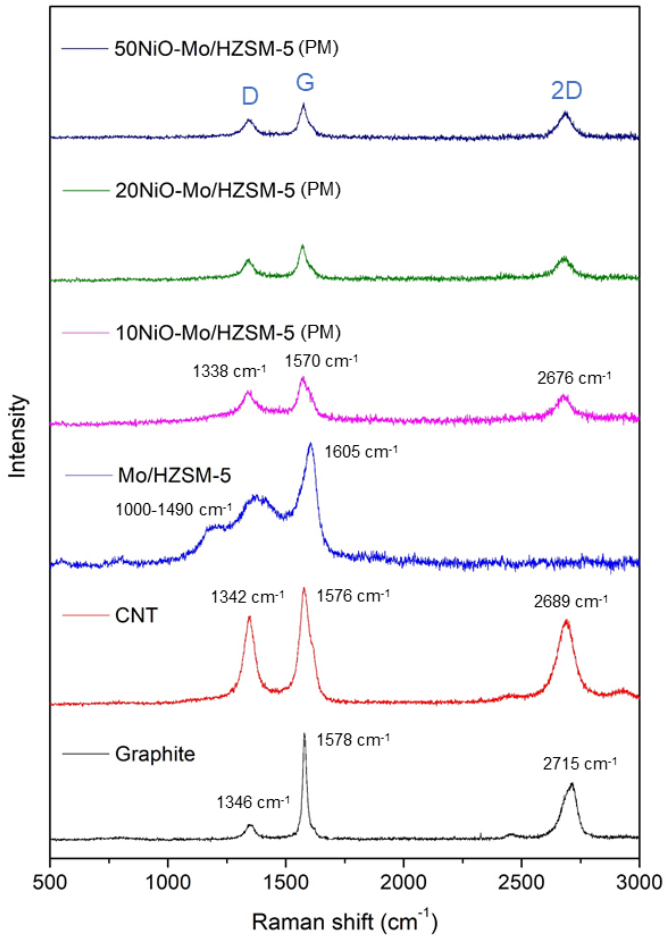

Fig. 2- 15. Raman spectra of graphite, CNT, and post-reaction catalysts.

2.3.3.3. Effect of NiO on textural properties of Mo/HZSM-5

Textural properties of the catalysts of pretreated and post-reaction catalysts were analyzed using N_2 physisorption. Table 2-6 shows that the surface area and micropore volume of the pretreated catalysts decreased gradually with increasing NiO content, because the content of zeolite reduced as NiO content increased. After the reaction, the surface area and micropore volume of all catalysts decreased, due to coke formation. However, the surface area and micropore volume of post-reaction NiO-Mo/HZSM-5(PM) was higher than those of post-reaction Mo/HZSM-5. Notably, post-reaction 10NiO-Mo/HZSM-5(PM) sample had the highest surface area of 169 m^2g^{-1}, and micropore volume of 0.07 cm^3g^{-1}. Furthermore, Mo/HZSM-5 had the highest relative decreased surface area of 64.9 %, while 10NiO-Mo/HZSM-5(PM) had the lowest of 23.4 %. In addition, the micropore volume of 10NiO-Mo/HZSM-5(PM) decreased by 21.0 %, whereas that of Mo/HZSM-5(PM) decreased by 82.6 %. N_2 isotherm in Fig. 2-16 also shows that Mo/HZSM-5 after pretreatment adsorbed largest volume of N_2, but it adsorbed smallest volume of N_2 after the reaction.

Fig. 2-17 shows the pore distribution of the pretreated and post-reaction catalysts. The main difference between the pretreated and post-reaction catalysts was observed in the pore size of 3.8 nm. It can be seen that when NiO was added, the mesopore of 3.8 nm was retained even after the reaction, whereas Mo/HZSM-5 lost its mesopore. Such evidence suggests that the addition of NiO inhibited the pore blockage of zeolite arising from coke

formation. In particular, the mesopore decreased marginally after the reaction over 10NiO-Mo/HZSM-5(PM). This means the pore of 10NiO-Mo/HZSM-5(PM) was less blocked than that of other catalysts, which is related to the highest catalytic stability.

Catalysts		BET surface area (m^2 g^{-1})	Micropore volume (cm^3 g^{-1})	Relative decreased surface area (%)	Relative decreased micropore volume (%)
Mo/HZSM-5	Pretreated	230	0.11	64.9	82.6
	Post-reaction	81	0.02		
10NiO-Mo/HZSM-5(PM)	Pretreated	220	0.09	23.4	21.0
	Post-reaction	169	0.07		
20NiO-Mo/HZSM-5(PM)	Pretreated	207	0.09	24.9	28.0
	Post-reaction	155	0.06		
50NiO-Mo/HZSM-5(PM)	Pretreated	160	0.06	28.4	19.8
	Post-reaction	114	0.05		

Table 2- 6. BET surface area and relative decreased surface area of the pretreated and post-reaction catalysts.

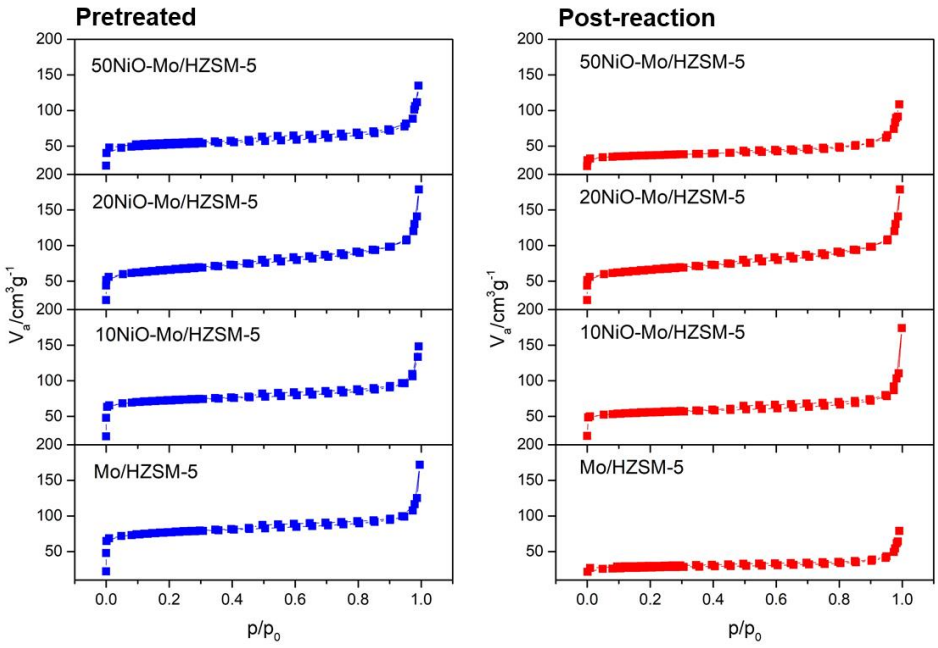

Fig. 2- 16. N_2 isotherm of the pretreated (left) and post-reaction (right), catalysts.

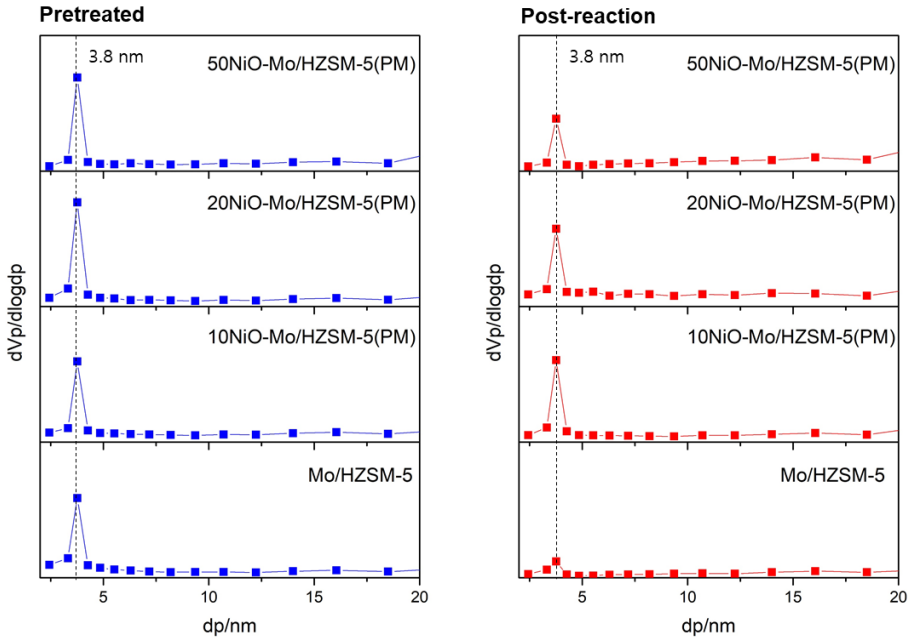

Fig. 2- 17. BJH pore distribution of the pretreated (left), and post-reaction (right), catalysts. All figures are displayed at identical scale.

2.3.4. Discussion

The MDA reaction results indicated that Mo/HZSM-5 physically mixed with NiO at up to 20 % Ni/Mo ratio enhanced both the CH_4 conversion and benzene yield. The CH_4–TPSR results clearly provide the evidence that the temperature where MoCx begins to form decreased over NiO-Mo/HZSM-5(PM). Lower reduction temperature restricted MoOx from agglomeration, resulting in higher dispersion of MoCx [38]. It is reported that well-dispersed MoCx formed at such lower temperature maintains higher activity with less agglomeration [55, 56]. This is consistent with the reaction results that the NiO-Mo/HZSM-5(PM) catalysts having MoCx, formed at lower temperature based on CH_4–TPSR, showed higher activity in the MDA reaction. CO chemisorption results, TEM images and acid distributions of the pretreated and post-reaction samples support this interpretation, which demonstrated higher dispersion of MoCx, as well as lower coke formation on Mo site and zeolite. The enhanced dispersion of MoCx results in increased CH_4 conversion and benzene yield, because of the increased amount of active Mo sites [37, 57]. To sum up, by mixing NiO physically with Mo/HZSM-5, highly dispersed MoCx formed at lower temperature, which resulted in enhanced catalytic activity.

Meanwhile, H_2 formation can affect the thermodynamic equilibrium of BTX formation because hydrogen is generated by dehydro-aromatization and its side reaction. H_2 production increased with increasing the content of

NiO. The thermodynamic equilibrium of benzene formation would have shifted to the left due to H_2 formation from coking. However, we propose that effect of enhanced dispersion is more dominant than that of equilibrium shift because overall CH_4 conversion and BTX yield were higher over 10NiO-Mo/HZSM-5(PM). Also, since Ni act as coke precursor scavenger, equilibrium between C2 hydrocarbon intermediates and BTX would have shifted to BTX, resulting in higher BTX yield.

Furthermore, NiO addition improved the catalytic stability. TEM showed that carbonaceous species was formed more dominantly on metallic Ni, rather than MoCx. Combined TPO and visible Raman analysis indicated that the addition of NiO gave rise to the reduced coke formation on Mo site and zeolite, at the expense of significant carbon nanotube formation on metallic Ni. In particular, visible Raman analysis showed that the amount of amorphous coke formed on Mo over NiO-Mo/HZSM-5(PM) was reduced. Meanwhile, the selectivity result from MDA reaction showed that NiO addition lowered the selectivity to naphthalene, the coke precursor. Sanapur et al. reported that amorphous coke on Mo/HZSM-5 consisted of polyaromatic coke, of which naphthalene was the main source [34]. Such previous study is consistent with the current visible Raman and selectivity result, indicating that low selectivity to naphthalene might lead to reduced amorphous coke formation. The BET surface areas and pore size distributions are in good agreement with the TPO and visible Raman analysis, demonstrating that the addition of NiO suppressed the micropore blockage in

zeolite arising from coke formation. In summary, NiO-Mo/HZSM-5(PM) produced coking dominantly on metallic Ni instead of on Mo site and zeolite, consequently enhancing the catalytic stability by protecting active sites.

Based on this study, two mechanisms for lower coke formation on Mo site and zeolite in NiO-Mo/HZSM-5(PM) sample can be suggested. Firstly, it has frequently been reported that catalytic stability could be affected by Mo dispersion [13, 14, 58]. When Mo is impregnated on the zeolite, Mo preferentially anchors to BAS that exists on the external surface, and inside zeolite channels [59]. Previous literature has reported that external BAS is the major coke deposition site [19]. If Mo dispersion increases, BAS that is present on the zeolite decreases, inhibiting coke formation [13, 58]. NH_3-TPD and pyridine FT-IR results in our study are in good agreement with previous literatures, implying that improved MoCx dispersion led to a decrease of BAS. Therefore, it can be claimed that improved Mo dispersion by NiO addition in NiO-Mo/HZSM-5(PM) sample has led to lower coke formation on BAS, extending the catalytic stability.

There is another factor for the slow deactivation rate of NiO-Mo/HZSM-5(PM). Metallic Ni could adsorb coke precursor to reduce coke formation on MoCx. The catalytic reaction results are also consistent with this proposal. If the CNT formation of the NiO-Mo/HZSM-5(PM) originated from the direct methane conversion on metallic Ni, methane conversion of NiO-Mo/HZSM-5(PM) with Ni/Mo ratio below 20 % would have increased with increase of the NiO content. However, there is not much difference in their

methane conversion. Therefore, in the case of NiO-Mo/HZSM-5(PM) catalysts with Ni/Mo ratio below 20 %, metallic Ni plays a crucial role in forming CNTs at the expense of coke precursors, rather than directly consuming methane.

In the case of Mo/HZSM-5, as mentioned above, the main cause of deactivation is the blocking of zeolite pores and the MoCx active sites with polyaromatic coke on the external surface [19, 34]. In contrast, in the case of NiO-Mo/HZSM-5(PM), metallic Ni inhibits the blockage of pores and the MoCx sites, by preventing agglomeration, and consuming the coke precursors during reaction resulting in the enhanced stability. Thus, the reactivity of MoCx site of NiO-Mo/HZSM-5(PM) is maintained with lower deactivation rate.

Chapter 3. Enhanced catalytic performance via introducing silica shell on physically mixed catalyst of Mo/HZSM−5 and NiO in methane dehydro−aromatization

3.1. Introduction

Natural gas or shale gas, which is mainly composed of methane, is promising alternative carbon source which can replace petroleum in the industry [1]. During combustion, it emits primarily carbon dioxide and water vapors, while coal and oil produce complex molecules containing high contents of nitrogen and sulfur, which give rise to the environmental pollution [2]. Considering the emission during the utilization, methane is the cleanest and most environmentally benign fossil fuel [2, 3]. Therefore, it is more environmentally friendly if the chemicals produced from fossil fuels can be obtained from methane. Besides, natural gas or shale gas is generally transported through pipelines, or in the form of liquefied natural gas (LNG). However, pipelines need expensive construction costs, and present the danger of leaks. Fugitive emissions of natural gas or shale gas during transportation are extremely concerned because of powerful greenhouse gas effect of methane [4]. Therefore, it is desirable to develop an efficient process to convert methane into more valuable hydrocarbon products, not only in terms of methane utilization, but also in terms of environmental friendliness [5].

However, methane utilization is challenging because of the high C-H activation energy of methane. The route for utilizing methane is divided into

indirect conversion, and direct conversion. In indirect conversion, methane is converted into syngas via reaction, such as steam reforming or partial oxidation; and then other hydrocarbons are produced from the syngas, via the Fischer–Tropsch process or methanol synthesis [6]. Such multi-step process results in high energy consumption. In contrast, by eliminating the intermediate syngas generation step, direct conversion has both energetic and economic advantages [7]. Direct conversion can be classified into oxidative reaction and non-oxidative reaction. Oxidative reaction can increase the reactivity of methane, although most methane is completely oxidized to CO_2 and H_2O [8]. Therefore, non-oxidative reaction is considered a more appropriate approach to increase the selectivity of the desired product. Among the alternative reactions, methane dehydro-aromatization (MDA) is one of the most attractive, because value-added chemicals, such as benzene, toluene, and xylene (BTX), are obtained as products, and can be used as feedstock chemicals in industry [9]. In addition, hydrogen, which is an essential feedstock for chemical industry, is produced with BTX during MDA.

Since Wang et al. first reported the MDA reaction for the production of benzene and hydrogen over Mo oxide supported on HZSM-5 (Mo/HZSM-5) at 700 °C [10], various metals supported on zeolite catalysts have been tested [11]. Previous studies concluded that the most promising catalysts for MDA were Mo supported on zeolites with pore diameters of 5–6 Å, such as ZSM-5, MCM-22, and ZSM-11 [12, 13]. The MDA reaction mechanism on Mo/HZSM-5 was reported to begin with carburization of the supported Mo

oxide to Mo oxycarbide or Mo carbide (MoCx) during the reaction [14, 15]. The Mo carbide species activates the C–H bond of methane, which is the rate determining step of MDA [16, 17]. C_2 intermediates derived from the activation of methane are oligomerized, to produce products such as benzene. During the MDA reaction, coke is also formed via additional reaction in the intermediate state, or excessive oligomerization in the product-like state [18]. The formation of coke, unwanted carbonaceous deposit, causes rapid deactivation of the Mo/HZSM-5 catalyst. In particular, the polyaromatic coke formed on the external surface of the zeolite has been regarded as the main deactivation factor among various carbonaceous deposits [19]. Therefore, the major issue in MDA reaction lies in how to increase methane activity, and prevent rapid deactivation arising from coke formation.

In order to improve the methane activity, as well as to inhibit deactivation, various approaches, such as promotor addition and pretreatment, have been undertaken. Although there are conflicting results among the research groups, the performance of the catalyst was enhanced when Fe [20, 21], Co [22, 23], Ni [24], Zn [21], Ga [25, 26], Ag [27], and P [28] were added as promotor. Tan showed that it was possible to increase the benzene yield and stability of Mo/HZSM-5 catalyst by using reaction gas (CH_4) during the pretreatment process [29]. In addition, metallic Ni has also been reported to have excellent methane dissociation ability [30].

Hence, in previous study, NiO was selected as a promoter, with anticipation that it could be converted to metallic Ni through the pretreatment

process, which was expected to help methane activation [60]. We prepared Mo/HZSM-5 samples physically mixed with NiO, followed by reductive pretreatment. We found that physically mixed catalysts showed better catalytic performance and stability than the impregnated one. In conclusion, the catalytic performance of Mo/HZSM-5 catalyst was enhanced by the use of bulk NiO, which is superior with respect to the simplicity and cost of synthesis procedure. In particular, previous study proposed two possible roles of NiO. First, improved Mo dispersion enhanced benzene yield. Second, metallic Ni converted coke precursors from Mo/HZSM-5 by growing CNT on itself. we further tried to elucidate the role of Ni in enhancing the activity and stability of MDA by investigating the physicochemical properties of the post-reaction samples. This study proposed two possible roles of NiO. First, improved Mo dispersion suppressed the deactivation of external BAS, as well as enhancing the benzene yield. Second, metallic Ni consumed coke precursors from Mo/HZSM-5 by growing CNT on itself.

However, our previous study confirmed that there was an optimum size for the particle size of NiO [61]. When the size of NiO particles was smaller than 36nm, NiO reacted with external MoOx to form $NiMoO_4$, causing agglomeration of Mo and delaying reduction, resulting in decreased activity. On the other hand, when the size was larger than 36nm, as the size of NiO decreased, catalytic activity was increased by leading to activation at lower temperatures [61]. Therefore, reducing the particle size of NiO to facilitate its reduction to metallic Ni, without reacting with external MoOx to

form $NiMoO_4$ at lower temperatures could also potentially lower the activation temperature of MoCx, thereby increasing catalytic activity. Hence, in this study, silica shell was introduced to NiO particles smaller than 36nm (nanoNiO) in order to prevent the reaction of NiO with external MoOx. In addition, bulk NiO, which was used previous study, was also coated with silica shell to compare the effect of silica shell. Ultimately, silica shell was introduced to NiO/SiO_2 in order to lower the size of NiO and use silica shell effect.

3.2. Experimental

3.2.1. Catalyst preparation

The core–shell structured NiO@SiO_2 samples were prepared by a modified Stöber method. Briefly, 0.4 g of bulk NiO or nano NiO (Sigma-Aldrich) was added to ethanol solution of 200 mL. After the solution was stirred for 12 h, $NH_3 \cdot H_2O$ (28 wt%) of 15 mL was added, and then the suspension was sonicated for 30 min. Subsequently, tetraethyl orthosilicate (TEOS, ⩾99%, Aldrich) of 0.3 mL was injected into the suspension. One hour later, the product was collected by centrifugation, washed twice with distilled water and ethanol, and dried at 80 °C in air for 10 h. Dried samples were calcined 4 h at 500 °C.

The core-shell structured SiO_2@NiO/SiO_2 samples were also prepared by a modified Stöber method. Briefly, silica nanosphere was synthesized by adding H_2O of 5.2 mL, $NH_3 \cdot H_2O$ (28 wt%) of 15 mL and TEOS of 7.6 mL to ethanol of 180mL. The ethanol solution was stirred overnight, and then the suspension was centrifuged and washed with distilled water and ethanol. Collected samples were dried at 80 °C in air for overnight. Synthesized silica nanospheres were added to ethanol (200mL ethanol/ g SiO_2 nanosphere) with 30min sonication to functionalization. After sonication, (3-Aminopropyl)trimethoxysilane (APTMS) of 0.1mL injected to solution with vigorous stirring. After 6 h, the product was collected by centrifugation, washed with ethanol. Collected samples were dried at 80 °C in air for

overnight. Functionalized silica nanosphere was added to ethanol and appropriate amount of ethanol solution of nickel nitrate hexahydrate (Alfa Aesar) were added. After 6 h stirring, the product was collected by evaporation and dried at 80 °C in air for overnight. Dried samples were calcined 0.5h at 450 °C (NiO/SiO_2). The obtained samples (NiO/SiO_2) were dispersed in ethanol by sonication. Appropriate amount of ethanol, H_2O, $NH_3 \cdot H_2O$ (28 wt%), TEOS were injected to solution with vigorous stirring. Six hours later, the product was centrifuged and washed with ethanol and distilled water. Dried samples were calcined at 2 h at 500 °C.

Commercial NH_4-ZSM-5 (Si/Al_2=23, Alfa Aesar) was used as the support of the catalysts. Commercial NH_4-ZSM-5 was calcined in a muffle furnace at 500 °C for 6 h to produce H-ZSM-5. H-ZSM-5 was impregnated with 12 wt.% of Mo by using aqueous solution of ammonium heptamolybdate tetrahydrate (Sigma-Aldrich). The resulting samples were dried at 105 °C overnight, and calcined in a furnace at 500 °C for 6 h. After the calcination, Mo/HZSM-5 and NiO (Sigma-Aldrich), NiO@SiO2, and SiO_2@NiO/SiO_2 were physically mixed for 10 min using mortar. Ni/Mo molar ratio of the physically mixed catalysts is fixed to 0.1.

3.2.2. Catalytic experiments

The MDA reaction was carried out over 0.2 g of the catalyst in a fixed-bed quartz reactor of 2 cm diameter and 50 cm length. The catalysts were crushed and sieved to 20–40 mesh. Catalyst samples were firstly activated in the reactor as a pretreatment process. The reactor was heated to 400 °C with a ramping rate of 20 °C/min, continuously heated to 700 °C at a ramping rate of 10 °C/min, and maintained for 10 min to stabilize temperature. Pretreatment gas was composed of 45 vol.% CH_4, 5 vol.% He, and 50 vol.% Ar, with a total flow rate of 20 mL/min. When the temperature was stabilized at 700 °C, the MDA reaction started by feeding 90 vol.% CH_4/He gas mixture to the reactor with a flow rate of 10 mL/min at atmospheric pressure. The effluent gases were analyzed at regular intervals by on-line gas chromatograph (YL6500GC) equipped with two columns (GS-Gaspro and Carboxen-1000 columns) and two detectors (flame ionization detector, and thermal conductivity detector). Ar was used as the carrier gas for GC. To prevent condensation and adsorption of the products, such as naphthalene, all the reactor outlet gas lines and gas sampling valves were maintained at 230 °C. Methane conversion and selectivity, and the yield of the carbon-containing products, were evaluated on the basis of carbon mass balance, by using He gas as an internal standard, as reported by Liu et al. [22].

3.2.3. Characterizations

The crystalline structure of the samples was obtained using powder X-ray diffraction (XRD). XRD was taken on a SmartLab (Rigaku) with Cu Kα radiation at 30 mA and 40 kV. The data was recorded at 2θ range of 5° to 80° with scanning step size of 0.02° at a speed of 2 °/min.

Temperature programmed surface reaction of methane (CH_4–TPSR) was carried out on fresh catalysts to identify the catalyst activation step by using a mass spectrometer (MS, Hiden Analytical). The sample was heated to 100 °C, and maintained for 1 h with 20 mL/min Ar gas to stabilize MS and remove water in the zeolite sample. Next, the gas was switched to 9 mL/min of CH_4, 1 mL/min of He, and 10 mL/min of Ar. The sample was heated to 300 °C at 10 °C/min, and consecutively heated to 900 °C at 2 °C/min. Intensities of H_2, CH_4, CO, Ar, and C_6H_6 were acquired by m/z value of 2, 16, 28, 40, and 78, respectively. Intensity of products was normalized by Ar in the feed.

Pulse CO chemisorption was conducted to compare exposed Mo sites present on the catalysts. Chemisorption measurements were done using BEL-CAT-II coupled with TCD (MicrotracBEL., Corp.) at 50 °C. Samples were pretreated in-situ with H_2 at 700 °C for 40 min since they were exposed to air before loading. A known volume of 4.98 % CO/He passed through a quartz reactor for 1 min. After equilibrium time for 10 min at atmospheric pressure, non-adsorbed CO was detected at the outlet of the reactor. CO pulse repeated

until the sample was completely saturated.

Transmission electron microscopy (TEM) and Energy dispersive spectroscopy (EDS) analysis was performed with an accelerating voltage of 200 kV in JEOL-2010 and JEM-ARM200F, respectively. Samples were prepared by dropping the suspension of sample diluted by ethanol on a Lacey-C Cu grid.

Visible Raman analysis of the post-reaction catalysts was performed to identify the carbonaceous deposit species present on the catalyst surface. Visible Raman spectra were recorded with a Renishaw (inVia™ Raman Microscope), equipped with CCD detector. The 532 nm line of a Nd:Yag laser was used as the excitation source.

Thermogravimetric analysis (TGA) was performed to quantify coke deposition on post-reaction catalysts. Post-reaction catalysts were loaded to a TGA N-1000 (Scinco) and heated to 800 °C with a ramping rate of 5 °C/min. Weight loss of post-reaction sample corresponding to coke removal was calculated with weight after water desorption.

3.3. Results and discussions

3.3.1. Catalyst synthesis results

Fig. 3-1 presents the TEM images of bulk NiO@SiO_2 and nano NiO@SiO_2. TEM images confirmed that both catalysts were well synthesized. Mean particle size of bulk NiO was 110 nm and nano NiO was 15 nm. Mean silica shell thickness of bulk NiO was 32 nm and nano NiO was 4 nm. It is general that the shell thickness increases in parallel with increasing core particle size [62]. The effect of silica shell on the activation step was investigated by comparing bulk NiO@SiO_2 and bulk NiO. Also, nano NiO@SiO_2 was intended to investigate whether NiO smaller than 36nm can be utilized through the introduction of silica shell.

Fig. 3-2 presents the TEM-EDS images of NiO/SiO_2. Mean particle size (diameter) of SiO_2 nanosphere was 96.7 nm and mean nanoparticle size of NiO was 5 nm. Also, EDS mapping image of Ni confirms that NiO was atomic-scale dispersed on functionalized SiO_2 and excess NiO formed nanoparticles.

Fig. 3-3 presents the TEM images of SiO_2@NiO/SiO_2. Mean particle size (diameter) of SiO_2 nanosphere was 105.2 nm and mean nanoparticle size of NiO was also 5.1 nm. Particle diameter difference between SiO_2@NiO/SiO_2 and NiO/SiO_2 confirms that mean shell thickness is 4.25 nm (105.2/2 - 96.7/2 = 4.25). Also, shell thickness measured through exposed

NiO nanoparticle was 4.1nm. Therefore, although distinguishing core and shell is difficult on TEM images since both core and shell are silica, it can be said that about 4 nm silica shell was uniformly formed.

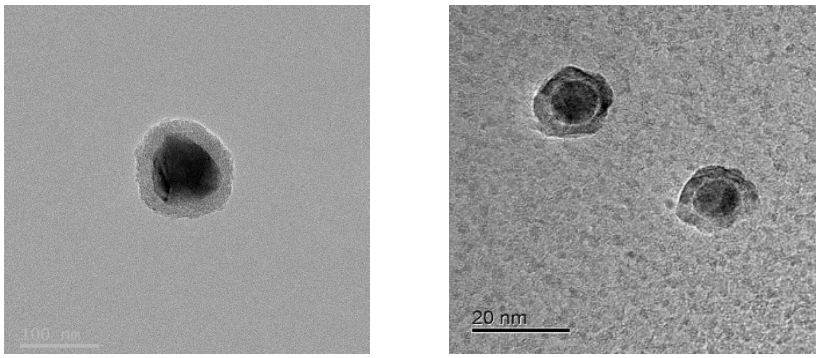

Fig. 3- 1. TEM images of bulk NiO@SiO_2 (left) and nano NiO@SiO_2 (right).

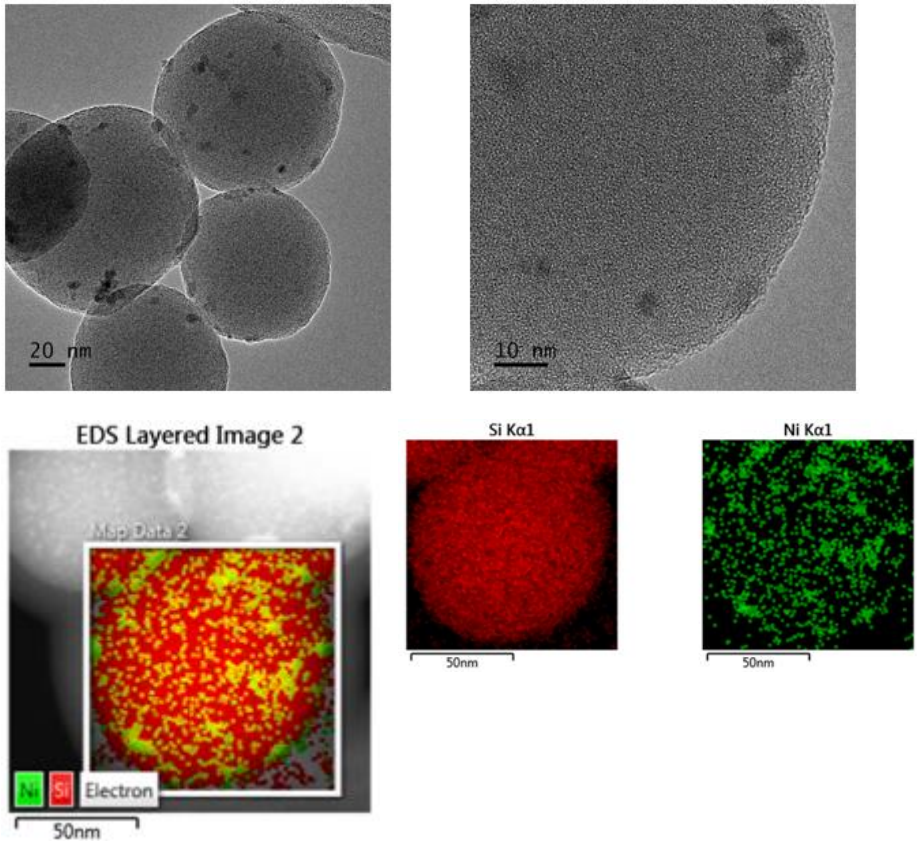

Fig. 3- 2. TEM-EDS images of NiO/SiO_2.

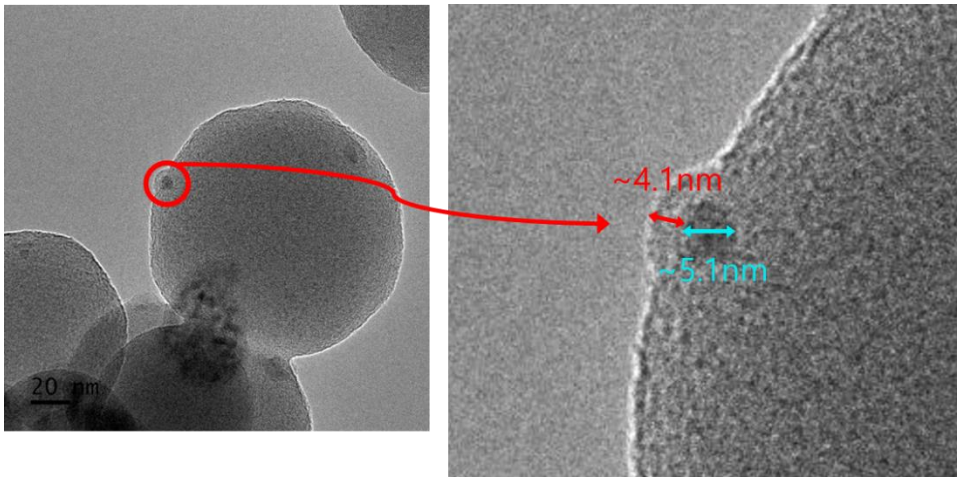

Fig. 3- 3. TEM images of SiO_2@NiO/SiO_2.

3.3.2. Methane dehydro-aromatization results

Fig. 3-4 represents the methane conversion and BTX yield obtained with time-on-stream (TOS) during MDA reaction over Mo/HZSM-5 with physically mixed catalysts. Several points should be noted in the catalytic reaction results.

First, bulkNiO@SiO_2-Mo/HZSM-5 showed the maximum BTX yield of 5.52%, which is similar to bulkNiO-Mo/HZSM-5 but slightly lower (maximum BTX yield of 5.6%). On the other hand, nanoNiO@SiO_2-Mo/HZSM-5 showed higher maximum BTX yield of 5.97%. Both Mo/HZSM-5 physically mixed with silica shell coated NiO catalysts showed better stability than Mo/HZSM-5, similar to bulkNiO-Mo/HZSM-5. This result implies that the promotion effect of physical mixing of NiO can occur even if silica shell is coated.

In contrast, SiO_2@NiO/SiO_2-Mo/HZSM-5 showed distinct differences compared to other physically mixed catalysts. SiO_2@NiO/SiO_2-Mo/HZSM-5 exhibited significantly higher maximum BTX yield of 7.20% and its deactivation rate was even similar to that of Mo/HZSM-5.

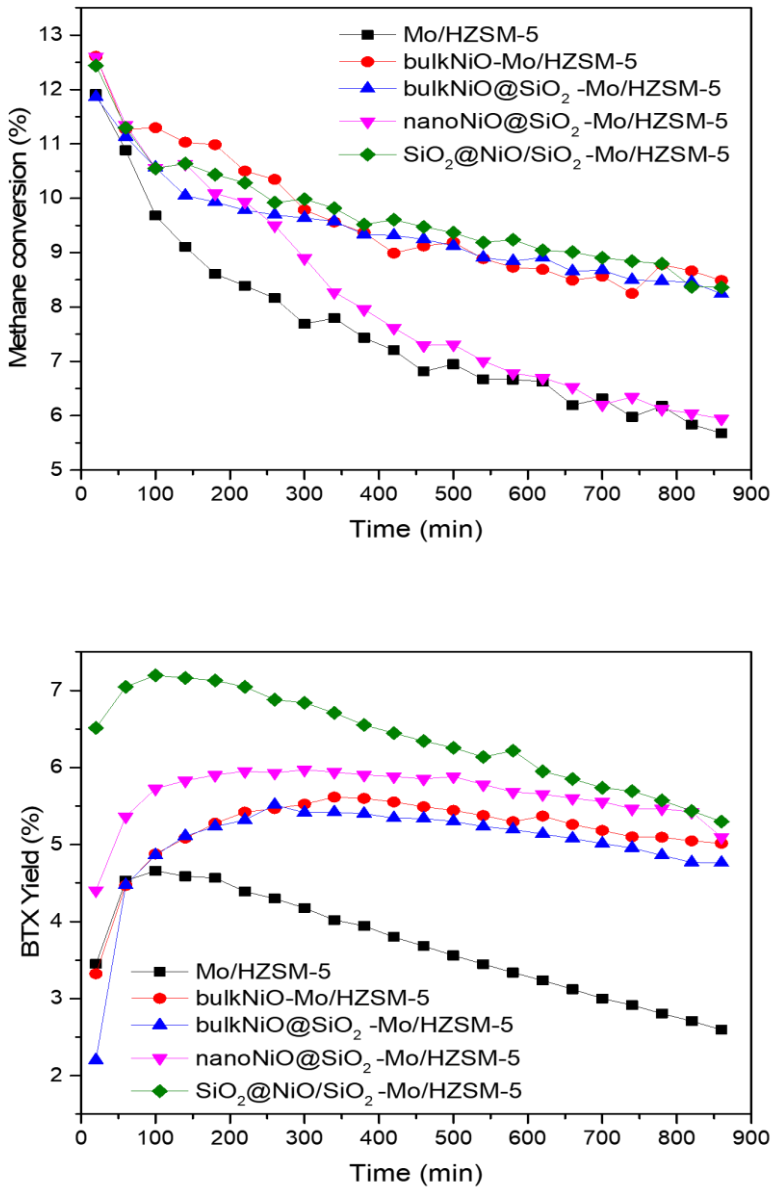

Fig. 3- 4. Catalytic performance of physically mixed catalysts with various Ni catalysts: Methane conversion (up), and BTX yield (down).

3.3.3. The effect of Silica shell on NiO

Fig. 3-5 show the XRD patterns of catalysts physically mixed with silica shell coated NiO. The XRD patterns of all samples match well with their supports, HZSM-5.

In the case of fresh catalysts, the peak at 2θ of 27.3° assigned to MoO_3 phase was detected. This means that even after the calcination, not all molybdenum oxide could be highly dispersed on the zeolite surface. Also, all fresh samples showed the peak arising from NiO phase, although silica shell is coated.

For pretreated catalysts, there was no peaks arising from Mo-related phase. This result implies that MoO_3 located on external surface were well carburized and dispersed. Also, peak arising from metallic Ni phase demonstrates that NiO was reduced to metallic Ni during pretreatment process even if NiO is coated with silica shell. In addition, there was no peak arising from Mo and Ni mixed crystallin phase.

In the case of post-reaction catalysts, peaks arising from metallic Ni and graphite-2H were obtained. Also, no peak corresponding to mixed Mo-Ni phases observed. The peak arising from metallic Ni indicates that metallic Ni initially formed by the pretreatment step was sustained during reaction process. In addition, as same as bulk NiO case, the graphite-2H peak can be interpreted to imply CNT formation [45, 60]. As mentioned, it is reported that Graphite-2H peak originates from carbon nanotube (CNT) [45], which are further analyzed by using TEM and visible Raman spectrometry.

Fig. 3-6 presents the CH_4-TPSR results of catalysts. During the pretreatment step, NiO and MoOx are reduced to metallic Ni and MoCx, respectively, as confirmed by XRD. The reduction sequence of these two oxides is expected to be clarified through CH_4–TPSR. Furthermore, the activation scheme of physically mixed catalysts during the MDA reaction can be understood by analyzing temperature where various products, such as H_2O, CO, and C_6H_6, begin to form.

Both physically mixed catalysts showed two peaks of H_2 and CO evolution. Based on the CH_4–TPSR results over bulk NiO and Mo/HZSM-5 in chapter 2, it can be claimed that the first evolution peaks of H_2 and CO are attributed to CH_4 decomposition during the reduction of NiO to metallic Ni, while the peaks at higher temperature are due to the reduction of MoOx to MoCx.

It was reported that migration of MoOx can occur above its Tammann temperature (534 K) because lattice mobility within MoO_3 becomes possible [38]. The CH_4–TPSR results clearly showed that MoCx was formed at relatively high temperature of 675 °C over Mo/HZSM-5, allowing MoOx to agglomerate with higher mobility and block zeolite pores before being reduced, thus forming a less dispersed MoCx. On the other hand, in case of bulkNiO-Mo/HZSM-5, metallic Ni helped MoOx to reduce at 633 °C, which was 40 °C lower than MoOx reduction temperature of Mo/HZSM-5. Lower reduction temperature allowed MoOx to have less mobility, resulting in higher dispersion of MoCx. These results confirm that metallic Ni facilitates

the reduction of MoOx, as well as the formation of MoCx, resulting in the promotion of benzene production. In addition, MoOx reduction temperature was 651 °C for bulkNiO@SiO_2-Mo/HZSM-5 and 615 °C for nanoNiO@SiO_2-Mo/HZSM-5. Through these results, it can be confirmed once again that the lowered MoOx reduction temperature increased reaction activity. Furthermore, Silica shell inhibited the MoOx activation in case of bulkNiO@SiO_2-Mo/HZSM-5, but also allowed NiO smaller than 36 nm to be utilized as promotor.

To sum up, these results suggest that methane reacts with NiO during the pretreatment step to form metallic Ni, and metallic Ni helps MoOx to be converted to MoCx with higher dispersion at lower temperature. To clarify this point, MoCx dispersion was further analyzed by CO chemisorption and TEM.

MoCx dispersion of pretreated and post-reaction catalysts were compared based on CO chemisorption (Table 3-1). Post reaction samples had less CO uptake than pretreated samples, which means that CO chemisorbed on coke were negligible. After the addition of bulk NiO, bulkNiO@SiO_2, and nanoNiO@SiO_2 by physical mixing, CO uptake of the pretreated catalysts increased from 0.19 cm^3g^{-1} to 0.64 cm^3g^{-1}, 0.62 cm^3g^{-1}, and 0.83 cm^3g^{-1}, In the case of post-reaction catalysts, CO uptake increased from 0.08 cm^3g^{-1} to 0.55 cm^3g^{-1}, 0.54 cm^3g^{-1}, and 0.60 cm^3g^{-1} after bulk NiO, bulkNiO@SiO_2, and nanoNiO@SiO_2 addition. Hence, it is confirmed that the catalysts showed lower activation temperature had more CO uptake, thus providing a

convincing evidence about higher MoCx dispersion.

Fig. 3-7 presents the TEM images of pretreated and post-reaction catalysts. Mean diameter of Mo particles calculated from TEM images also confirmed that the catalysts showed lower activation temperature had higher MoCx dispersion.

In addition, large amount of carbon nanotube (CNT) could be seen on the post-reaction catalysts on TEM image. These results are in line with graphite-2H peak at XRD patterns and visible Raman spectrometry (Fig. 3-12).

In conclusion, in the case of bulkNiO@SiO_2-Mo/HZSM-5, 32nm thickness silica shell suppressed the activation of MoOx compared to bulkNiO-Mo/HZSM-5. On the other hand, in the case of nanoNiO@SiO_2-Mo/HZSM-5, 4nm thickness silica shell allowed NiO smaller than 36nm to act as promotor. As such, it was confirmed that the promoting effect of NiO can be maintained through introducing silica shell. However, it is reasonable that not only the shell existence but also the thickness of the silica shell affects the activation step. Therefore, it can be predicted that the catalytic activity can be further enhanced by using smaller size NiO and shell with appropriate thickness. The way to verify this hypothesis is using SiO_2@NiO/SiO_2 structure with shell thickness is 4nm, which is verified by nanoNiO@SiO_2-Mo/HZSM-5.

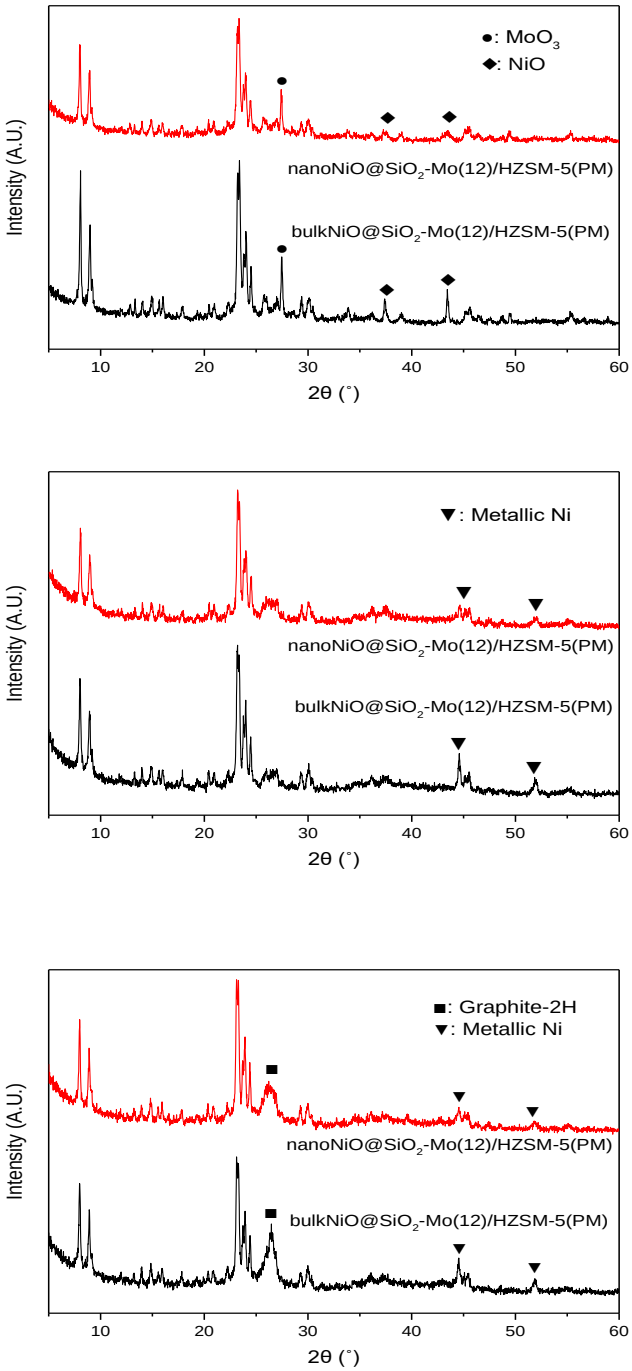

Fig. 3- 5. XRD patterns of bulk NiO@SiO_2 and nano NiO@SiO_2 physically mixed catalysts (fresh, pretreated, post-reaction).

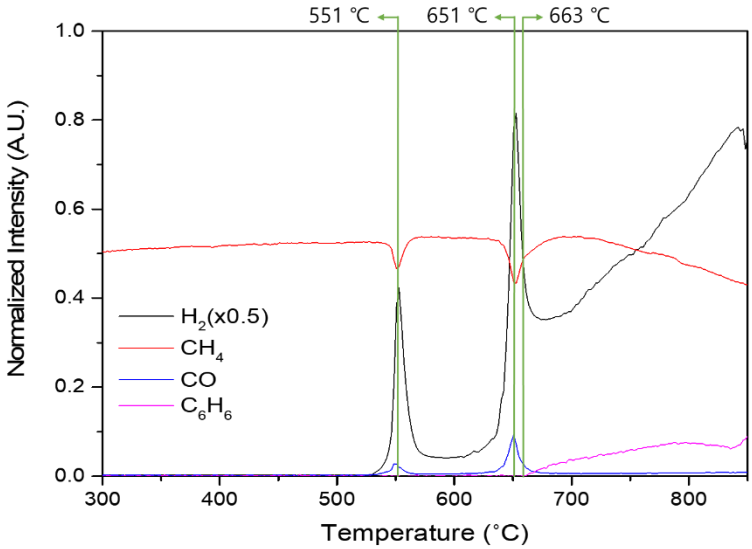

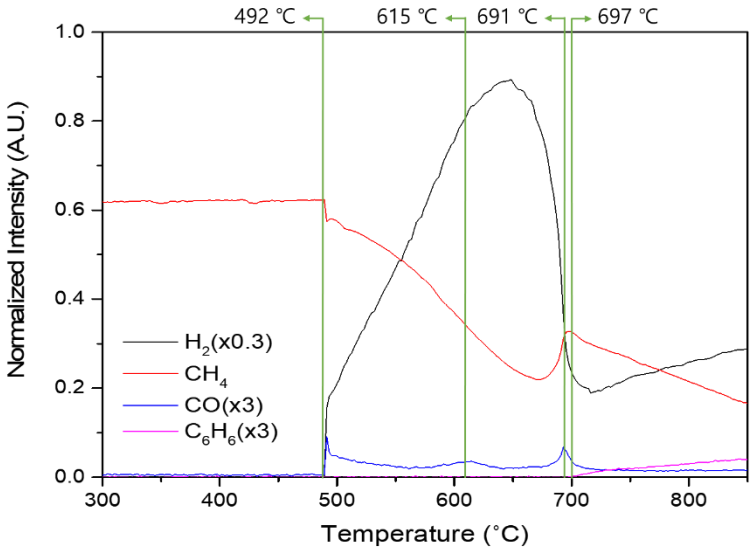

Fig. 3- 6. CH_4–TPSR profiles of bulk NiO@SiO_2-Mo/HZSM-5 (up), and nanoNiO@SiO_2-Mo/HZSM-5 (down)

	Catalysts	CO uptake (cm^3g^{-1})[a]
Pretreated	Mo/HZSM-5	0.19
	10NiO-Mo/HZSM-5(PM)	0.64
	Bulk NiO@SiO_2-Mo/HZSM-5(PM)	0.62
	Nano NiO@SiO_2-Mo/HZSM-5(PM)	0.83
	SiO_2@NiO/SiO_2-Mo/HZSM-5(PM)	0.91
Post-reaction	Mo/HZSM-5	0.08
	10NiO-Mo/HZSM-5(PM)	0.55
	Bulk NiO@SiO_2-Mo/HZSM-5(PM)	0.54
	Nano NiO@SiO_2-Mo/HZSM-5(PM)	0.60
	SiO_2@NiO/SiO_2-Mo/HZSM-5(PM)	0.61

Table 3- 1. CO uptake over pretreated and post-reaction catalysts.

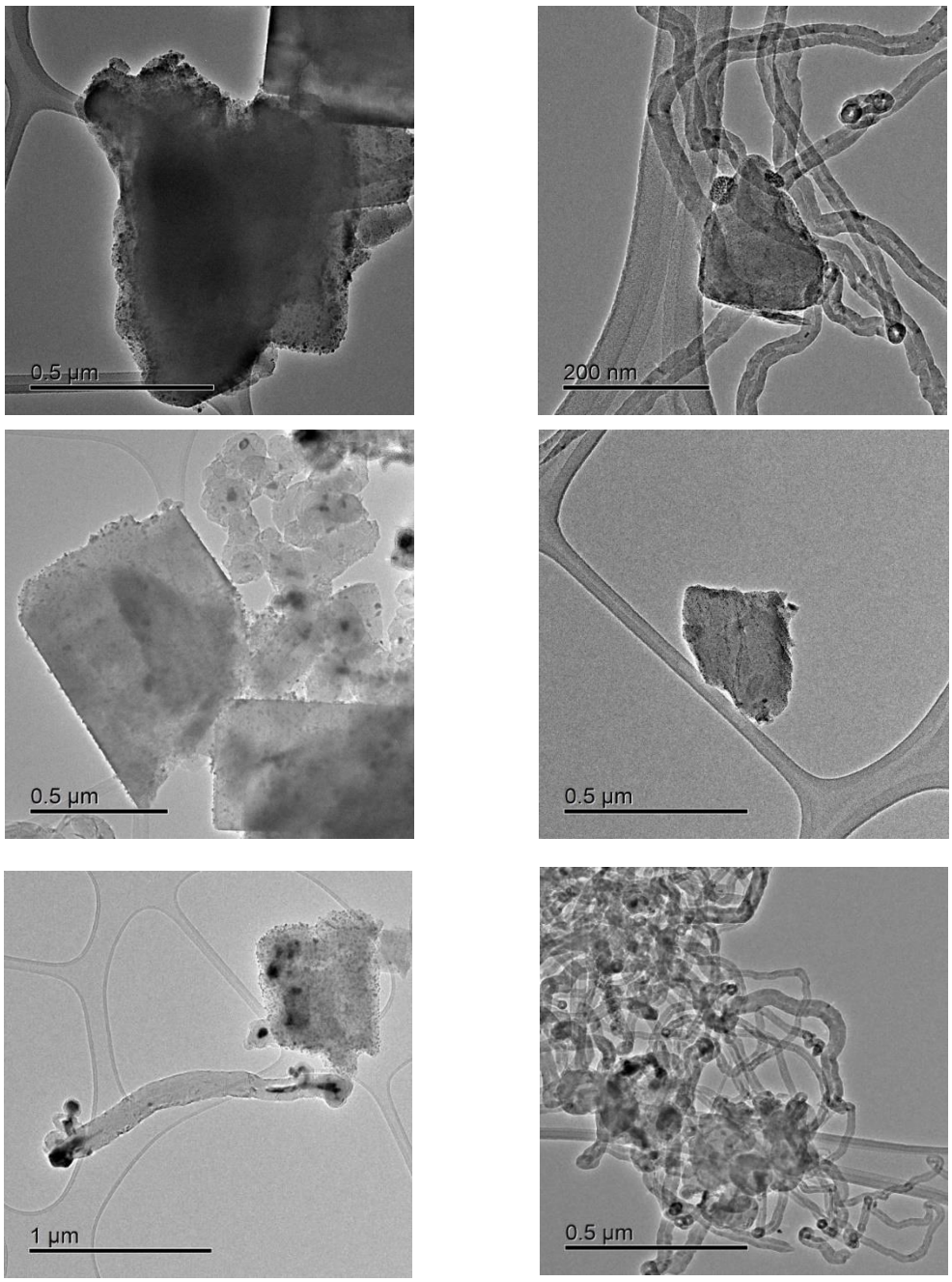

Fig. 3- 7. TEM images of of pretreated (up 1) and post-reaction (down 2) bulk NiO@SiO2-Mo/HZSM-5 (left), and nanoNiO@SiO2-Mo/HZSM-5 (right).

3.3.4. The effect of Silica shell and smaller NiO particle size by using NiO/SiO_2

Fig. 3-8 show the XRD patterns of SiO_2@NiO/SiO_2-Mo/HZSM-5. The XRD patterns of all samples match well with their supports, HZSM-5.

In the case of fresh catalysts, the peak at 2θ of 27.3° assigned to MoO_3 phase was detected. This means that even after the calcination, not all molybdenum oxide could be highly dispersed on the zeolite surface. Also, all fresh samples showed the peak arising from NiO phase, although silica shell is coated.

For pretreated catalysts, there was no peaks arising from Mo-related phase. This result implies that MoO_3 located on external surface were well carburized and dispersed. Also, peak arising from metallic Ni phase demonstrates that NiO was reduced to metallic Ni during pretreatment process even if NiO is coated with silica shell. In addition, there was no peak arising from Mo and Ni mixed crystallin phase.

In the case of post-reaction catalysts, peaks arising from metallic Ni were observed. Also, no peak corresponding to graphite-2H and mixed Mo-Ni phases observed. The peak arising from metallic Ni indicates that metallic Ni initially formed by the pretreatment step was sustained during reaction process. In addition, unlike the previous cases, the absence of graphite-2H peak can be as less CNT formation during reaction. As mentioned, it is reported that Graphite-2H peak originates from carbon nanotube (CNT) [45], which are further analyzed by using TEM and visible Raman spectrometry.

Fig. 3-9 presents the CH_4-TPSR results of catalysts. During the pretreatment step, NiO and MoOx are reduced to metallic Ni and MoCx, respectively, as confirmed by XRD. The reduction sequence of these two oxides is expected to be clarified through CH_4–TPSR. Furthermore, the activation scheme of physically mixed catalysts during the MDA reaction can be understood by analyzing temperature where various products, such as H_2O, CO, and C_6H_6, begin to form.

Physically mixed catalysts showed one peaks of H_2 and CO evolution. Based on the CH_4–TPSR results over bulk NiO and Mo/HZSM-5 in chapter 2, it can be claimed that the start point of the peak of H_2 and CO is attributed to CH_4 decomposition during the reduction of NiO to metallic Ni, while the peaks at higher temperature are due to the reduction of MoOx to MoCx.

It was reported that migration of MoOx can occur above its Tammann temperature (534 K) because lattice mobility within MoO_3 becomes possible [38]. The CH_4–TPSR results clearly showed that MoCx was formed at relatively high temperature of 675 °C over Mo/HZSM-5, allowing MoOx to agglomerate with higher mobility and block zeolite pores before being reduced, thus forming a less dispersed MoCx. On the other hand, in case of SiO_2@NiO/SiO_2-Mo/HZSM-5, metallic Ni helped MoOx to reduce at 591 °C, which was 84 °C lower than MoOx reduction temperature of Mo/HZSM-5. Lower reduction temperature allowed MoOx to have less mobility, resulting in higher dispersion of MoCx. These results confirm that metallic Ni facilitates the reduction of MoOx, as well as the formation of MoCx, resulting

in the promotion of benzene production. Through these results, it can be confirmed once again that the lowered MoOx reduction temperature increased reaction activity.

To sum up, these results suggest that methane reacts with NiO during the pretreatment step to form metallic Ni, and metallic Ni helps MoOx to be converted to MoCx with higher dispersion at lower temperature. To clarify this point, MoCx dispersion was further analyzed by CO chemisorption.

MoCx dispersion of pretreated and post-reaction catalysts were compared based on CO chemisorption (Table 3-1). Post reaction samples had less CO uptake than pretreated samples, which means that CO chemisorbed on coke were negligible. After the addition of SiO_2@NiO/SiO_2 by physical mixing, CO uptake of the pretreated catalysts increased from 0.19 cm^3g^{-1} to 0.91 cm^3g^{-1}, In the case of post-reaction catalysts, CO uptake increased from 0.08 cm^3g^{-1} to 0.61 cm^3g^{-1} after SiO_2@NiO/SiO_2 addition. Hence, it is confirmed that the catalysts showed lower activation temperature had more CO uptake, thus providing a convincing evidence about higher MoCx dispersion.

Fig. 3-10, 11 presents the TEM images of pretreated and post-reaction catalysts. It can be confirmed that CNT formation is less than other physically mixed catalysts mentioned in previous section. These results are in line with absence of graphite-2H peak at XRD patterns and visible Raman spectrometry (Fig. 3-12). In addition, when focused on Ni/SiO_2 side, Ni aggregates less than other physically mixed catalysts. This results implies

lower exposure of Ni than other physically mixed samples.

In conclusion, SiO_2@NiO/SiO_2-Mo/HZSM-5 utilizing appropriate shell thickness and smaller NiO allowed further enhancement of catalytic activity. However, deactivation rate was similar to Mo/HZSM-5 because the exposure of Ni was less than other physically mixed catalysts, resulting in more polyaromatic coke formation than CNT formation.

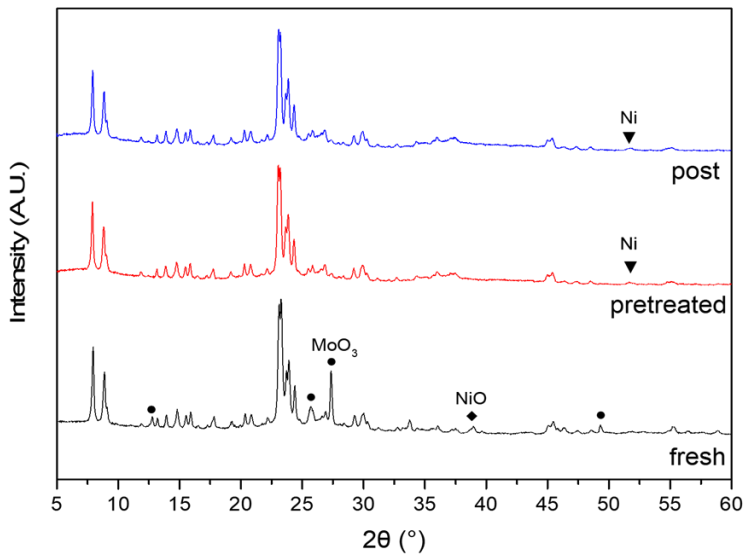

Fig. 3- 8. XRD patterns of SiO_2@NiO/SiO_2-Mo/HZSM-5.

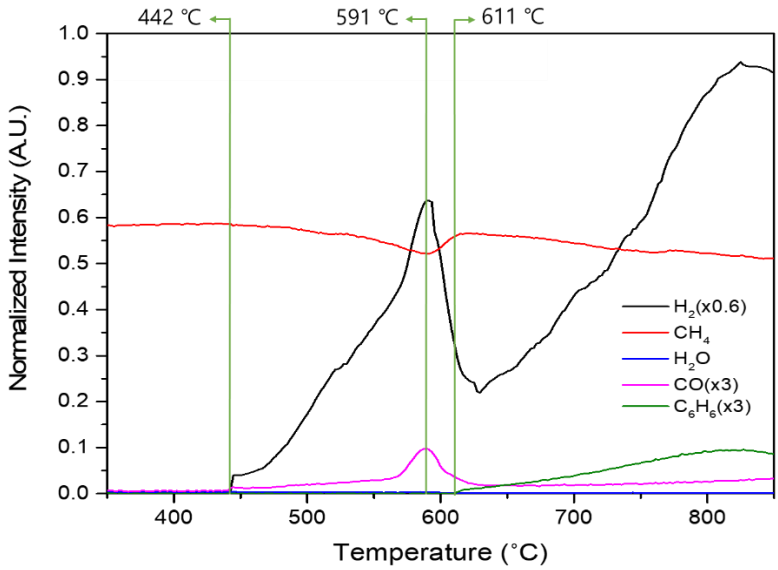

Fig. 3- 9. CH_4–TPSR profiles of SiO_2@NiO/SiO_2-Mo/HZSM-5.

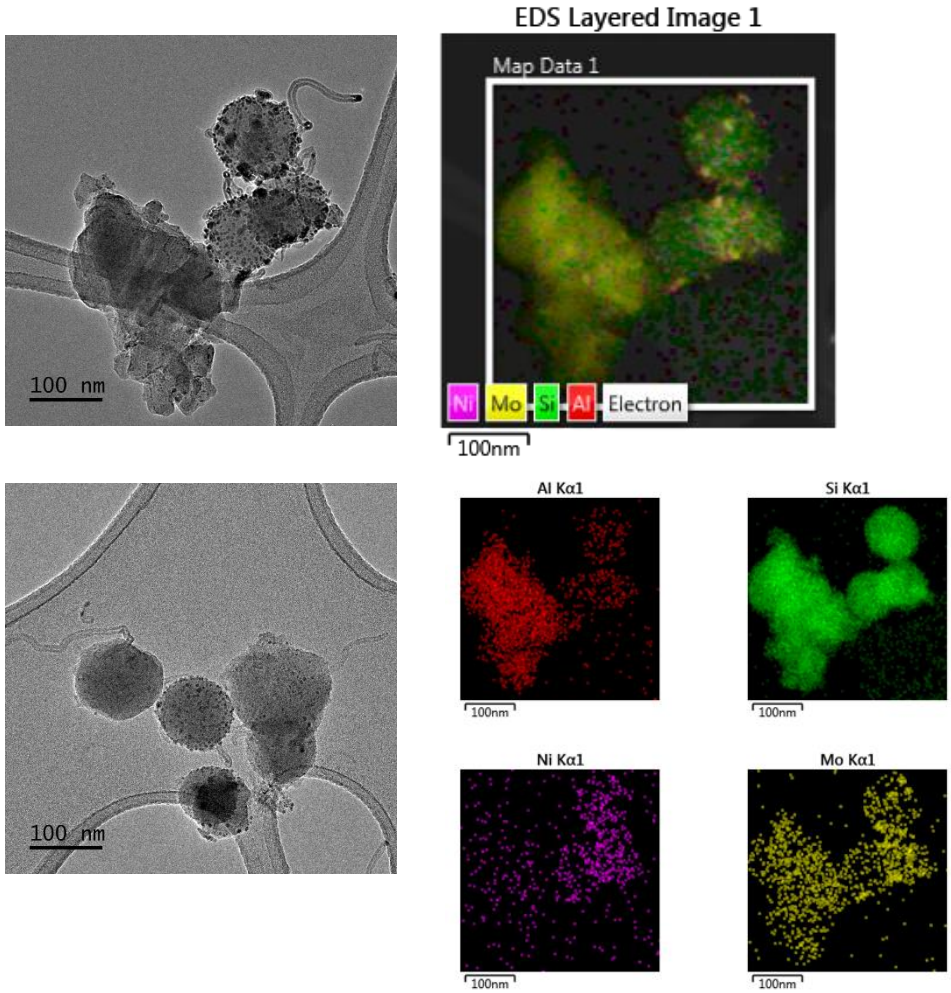

Fig. 3- 10. TEM-EDS images of pretreated SiO_2@NiO/SiO_2-Mo/HZSM-5.

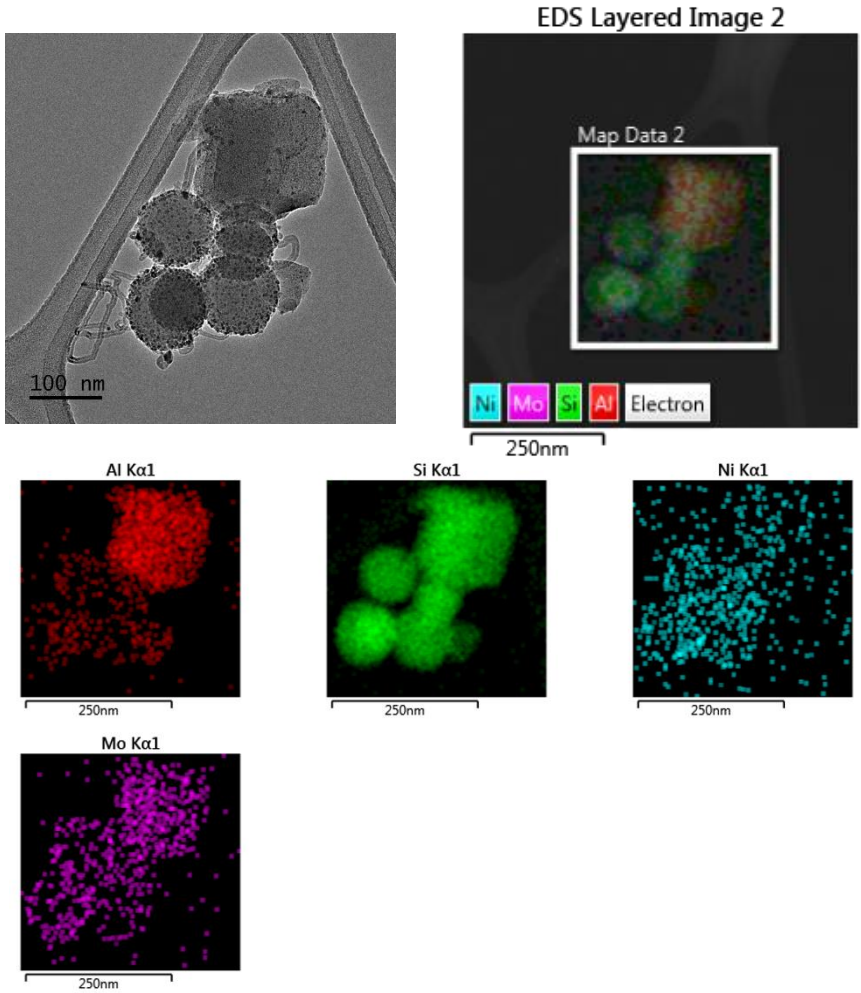

Fig. 3- 11. TEM-EDS images of post-reaction SiO_2@NiO/SiO_2-Mo/HZSM-5.

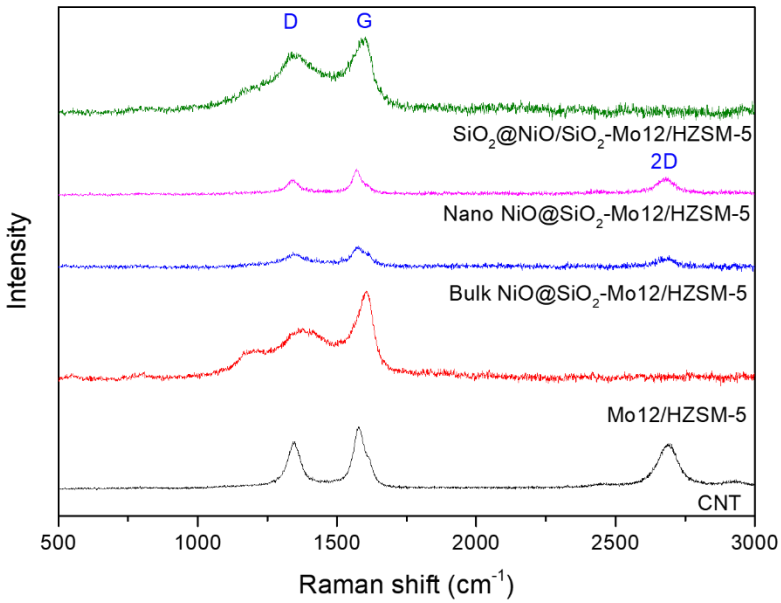

Fig. 3- 12. Raman spectra of CNT and post-reaction catalysts.

Chapter 4. Conclusions and summary

Although NiO-Mo/HZSM-5(IMP) showed no significant improvement on catalytic reaction, NiO-Mo/HZSM-5(PM) up to 20 % Ni/Mo ratio significantly improved both the catalytic activity and stability. In particular, 10NiO-Mo/HZSM-5(PM) had the highest BTX yield with enhanced stability. Metallic Ni decreased the temperature where MoCx phase begins to form, resulting in enhanced MoCx dispersion and benzene production. Although the amount of carbon species increased with increasing NiO content, the amount of coke formed on the Mo site and zeolite decreased. It was recognized that metallic Ni inhibited coke formation on the Mo site and zeolite by growing CNT on itself. This study proposed two possible roles of NiO. First, improved MoCx dispersion suppressed the deactivation of external BAS, as well as enhancing the benzene yield. Second, metallic Ni consumed coke precursors from Mo/HZSM-5 by growing CNT on itself.

In addition, the presence of silica shells on NiO ($NiO@SiO_2$) was also found to promote MoCx dispersion by altering activation temperature of MoCx, but the shells were broken, resulting in the formation of CNTs similarly to bare NiO. In the case of silica shells on NiO/SiO_2 ($SiO_2@NiO/SiO_2$) also, the catalytic activity was enhanced by improved MoCx dispersion. On the contrary, metallic Ni exposure did not occur as much as bare NiO, resulting in less formation of CNTs, a different deactivation trend was observed. In conclusion, this study demonstrates that

physically mixed NiO and appropriate introducing silica shell and controlling particle size for NiO can further enhance the catalytic activity for MDA as promotor.

Bibliography

[1] W. Taifan, J. Baltrusaitis, CH4 conversion to value added products: Potential, limitations and extensions of a single step heterogeneous catalysis, Applied Catalysis B: Environmental, 198 (2016) 525-547.
[2] S.N. Malik, O.R. Sukhera, Management of natural gas resources and search for alternative renewable energy resources: A case study of Pakistan, Renewable and Sustainable Energy Reviews, 16 (2012) 1282-1290.
[3] M.P. Hekkert, F.H.J.F. Hendriks, A.P.C. Faaij, M.L. Neelis, Natural gas as an alternative to crude oil in automotive fuel chains well-to-wheel analysis and transition strategy development, Energy Policy, 33 (2005) 579-594.
[4] R.W. Howarth, R. Santoro, A. Ingraffea, Methane and the greenhouse-gas footprint of natural gas from shale formations, Climatic Change, 106 (2011) 679.
[5] J. Gao, Y. Zheng, J.-M. Jehng, Y. Tang, I.E. Wachs, S.G. Podkolzin, Identification of molybdenum oxide nanostructures on zeolites for natural gas conversion, Science, 348 (2015) 686-690.
[6] S. Majhi, P. Mohanty, H. Wang, K.K. Pant, Direct conversion of natural gas to higher hydrocarbons: A review, Journal of Energy Chemistry, 22 (2013) 543-554.
[7] J.H. Lunsford, Catalytic conversion of methane to more useful chemicals and fuels: a challenge for the 21st century, Catalysis Today, 63 (2000) 165-174.
[8] S. Ma, X. Guo, L. Zhao, S. Scott, X. Bao, Recent progress in methane dehydroaromatization: From laboratory curiosities to promising technology, Journal of Energy Chemistry, 22 (2013) 1-20.
[9] N. Kosinov, A.S.G. Wijpkema, E. Uslamin, R. Rohling, F.J.A.G. Coumans, B. Mezari, A. Parastaev, A.S. Poryvaev, M.V. Fedin, E.A. Pidko, E.J.M. Hensen, Confined Carbon Mediating Dehydroaromatization of Methane over Mo/ZSM-5, Angewandte Chemie - International Edition, 57 (2018) 1016-1020.
[10] L. Wang, L. Tao, M. Xie, G. Xu, J. Huang, Y. Xu, Dehydrogenation and aromatization of methane under non-oxidizing conditions, Catalysis Letters, 21 (1993) 35-41.
[11] P. Schwach, X. Pan, X. Bao, Direct Conversion of Methane to Value-Added Chemicals over Heterogeneous Catalysts: Challenges and Prospects, Chemical Reviews, 117 (2017) 8497-8520.
[12] Z.R. Ismagilov, E.V. Matus, L.T. Tsikoza, Direct conversion of methane on Mo/ZSM-5 catalysts to produce benzene and hydrogen: achievements and perspectives, Energy & Environmental Science, 1 (2008) 526.
[13] T.H. Lim, K. Nam, I.K. Song, K.-Y. Lee, D.H. Kim, Effect of Si/Al2 ratios in Mo/H-MCM-22 on methane dehydroaromatization, Applied Catalysis A: General, 552 (2018) 11-20.
[14] N. Kosinov, F.J.A.G. Coumans, G. Li, E. Uslamin, B. Mezari, A.S.G. Wijpkema, E.A. Pidko, E.J.M. Hensen, Stable Mo/HZSM-5 methane dehydroaromatization catalysts optimized for high-temperature calcination-regeneration, Journal of Catalysis, 346 (2017) 125-133.
[15] N. Kosinov, E.J.M. Hensen, Reactivity, Selectivity, and Stability of Zeolite-Based Catalysts for Methane Dehydroaromatization, Adv. Mater., 32 (2020) 2002565.
[16] D. Zhou, S. Zuo, S. Xing, Methane Dehydrogenation and Coupling to Ethylene over a Mo/HZSM-5 Catalyst: A Density Functional Theory Study, The Journal of Physical Chemistry C, 116 (2012) 4060-4070.
[17] D. Kiani, S. Sourav, Y. Tang, J. Baltrusaitis, I.E. Wachs, Methane activation by ZSM-5-supported transition metal centers, Chemical Society Reviews, (2021).
[18] J.J. Spivey, G. Hutchings, Catalytic aromatization of methane, Chemical Society Reviews, 43 (2014) 792-803.
[19] C.H.L. Tempelman, E.J.M. Hensen, On the deactivation of Mo/HZSM-5 in the methane dehydroaromatization reaction, Appl. Catal. B: Environ., 176-177 (2015) 731-739.
[20] Y. Xu, J. Wang, Y. Suzuki, Z.-G. Zhang, Improving effect of Fe additive on the catalytic

stability of Mo/HZSM-5 in the methane dehydroaromatization, Catalysis today, 185 (2012) 41-46.
[21] V. Abdelsayed, D. Shekhawat, M.W. Smith, Effect of Fe and Zn promoters on Mo/HZSM-5 catalyst for methane dehydroaromatization, Fuel, 139 (2015) 401-410.
[22] S. Liu, Q. Dong, R. Ohnishi, M. Ichikawa, Remarkable non-oxidative conversion of methane to naphthalene and benzene on Co and Fe modified Mo/HZSM-5 catalysts, Chemical Communications, (1997) 1455-1456.
[23] A.K. Aboul-Gheit, M.S. El-Masry, A.E. Awadallah, Oxygen free conversion of natural gas to useful hydrocarbons and hydrogen over monometallic Mo and bimetallic Mo–Fe, Mo–Co or Mo–Ni/HZSM-5 catalysts prepared by mechanical mixing, Fuel Processing Technology, 102 (2012) 24-29.
[24] A.V. Vosmerikov, V.I. Zaikovskii, L.L. Korobitsyna, G.V. Echevskii, V.V. Kozlov, Y.E. Barbashin, S.P. Zhuravkov, Nonoxidative conversion of methane into aromatic hydrocarbons on Ni-Mo/ZSM-5 catalysts, Kinetics and Catalysis, 50 (2009) 725.
[25] B. Liu, Y. Yang, A. Sayari, Non-oxidative dehydroaromatization of methane over Ga-promoted Mo/HZSM-5-based catalysts, Applied Catalysis A: General, 214 (2001) 95-102.
[26] B.S. Liu, L. Jiang, H. Sun, C.T. Au, XPS, XAES, and TG/DTA characterization of deposited carbon in methane dehydroaromatization over Ga–Mo/ZSM-5 catalyst, Applied Surface Science, 253 (2007) 5092-5100.
[27] M.W. Ngobeni, A.F. Carley, M.S. Scurrell, C.P. Nicolaides, The effects of boron and silver on the oxygen-free conversion of methane over Mo/H-ZSM-5 catalysts, Journal of Molecular Catalysis A: Chemical, 305 (2009) 40-46.
[28] S. Burns, J.S.J. Hargreaves, P. Pal, K.M. Parida, S. Parija, The effect of dopants on the activity of MoO3/ZSM-5 catalysts for the dehydroaromatisation of methane, Catalysis Today, 114 (2006) 383-387.
[29] P. Tan, The catalytic performance of Mo-impregnated HZSM-5 zeolite in CH4 aromatization: Strong influence of Mo loading and pretreatment conditions, Catalysis Communications, 103 (2018) 101-104.
[30] Y. Shen, A.C. Lua, Synthesis of Ni and Ni–Cu supported on carbon nanotubes for hydrogen and carbon production by catalytic decomposition of methane, Applied Catalysis B: Environmental, 164 (2015) 61-69.
[31] A. Sridhar, M. Rahman, A. Infantes-Molina, B.J. Wylie, C.G. Borcik, S.J. Khatib, Bimetallic Mo-Co/ZSM-5 and Mo-Ni/ZSM-5 catalysts for methane dehydroaromatization: A study of the effect of pretreatment and metal loadings on the catalytic behavior, Appl. Catal. A: Gen., 589 (2020) 117247.
[32] I. Vollmer, E. Abou-Hamad, J. Gascon, F. Kapteijn, Aromatization of Ethylene – Main Intermediate for MDA?, ChemCatChem, 12 (2020) 544-549.
[33] N. Kosinov, E.A. Uslamin, F.J.A.G. Coumans, A.S.G. Wijpkema, R.Y. Rohling, E.J.M. Hensen, Structure and Evolution of Confined Carbon Species during Methane Dehydroaromatization over Mo/ZSM-5, ACS Catalysis, 8 (2018) 8459-8467.
[34] G. Sanapur, A. Kumar, A. Mondal, S. Sreeramagiri, R. Dongara, G. Ramaswamy, Thermal desorption and characterization of carbonaceous deposits in Mo/HZSM-5 catalyst, Journal of Analytical and Applied Pyrolysis, 138 (2019) 22-28.
[35] B. Li, S. Li, N. Li, H. Chen, W. Zhang, X. Bao, B. Lin, Structure and acidity of Mo/ZSM-5 synthesized by solid state reaction for methane dehydrogenation and aromatization, Microporous and Mesoporous Materials, 88 (2006) 244-253.
[36] H. Liu, X. Bao, Y. Xu, Methane dehydroaromatization under nonoxidative conditions over Mo/HZSM-5 catalysts: Identification and preparation of the Mo active species, J. Catal., 239 (2006) 441-450.
[37] D. Wang, J.H. Lunsford, M.P. Rosynek, Characterization of a Mo/ZSM-5 Catalyst for the Conversion of Methane to Benzene, J. Catal., 169 (1997) 347-358.
[38] R.W. Borry, Y.H. Kim, A. Huffsmith, J.A. Reimer, E. Iglesia, Structure and Density of Mo and Acid Sites in Mo-Exchanged H-ZSM5 Catalysts for Nonoxidative Methane Conversion, The Journal of Physical Chemistry B, 103 (1999) 5787-5796.

[39] N. Kosinov, E.A. Uslamin, L. Meng, A. Parastaev, Y. Liu, E.J.M. Hensen, Reversible Nature of Coke Formation on Mo/ZSM-5 Methane Dehydroaromatization Catalysts, Angewandte Chemie - International Edition, 58 (2019) 7068-7072.
[40] J. Gao, Y. Zheng, G.B. Fitzgerald, J. de Joannis, Y. Tang, I.E. Wachs, S.G. Podkolzin, Structure of Mo2C x and Mo4C x Molybdenum Carbide Nanoparticles and Their Anchoring Sites on ZSM-5 Zeolites, The Journal of Physical Chemistry C, 118 (2014) 4670-4679.
[41] A.V. Vasilevich, O.N. Baklanova, A.V. Lavrenov, O.A. Knyazheva, T.I. Gulyaeva, M.V. Trenikhin, V.A. Likholobov, Synthesis and characterization of massive molybdenum carbides and supported carbide-containing catalysts Mo2C/C prepared through mechanical activation, Catalysis in Industry, 6 (2014) 8-16.
[42] A.S. Al-Dughaither, H. de Lasa, HZSM-5 Zeolites with Different SiO2/Al2O3 Ratios. Characterization and NH3 Desorption Kinetics, Industrial & Engineering Chemistry Research, 53 (2014) 15303-15316.
[43] C.A. Emeis, Determination of Integrated Molar Extinction Coefficients for Infrared Absorption Bands of Pyridine Adsorbed on Solid Acid Catalysts, Journal of Catalysis, 141 (1993) 347-354.
[44] F. Lónyi, J. Valyon, On the interpretation of the NH3-TPD patterns of H-ZSM-5 and H-mordenite, Microporous and Mesoporous Materials, 47 (2001) 293-301.
[45] B. Escobar, R. Barbosa, M. Miki Yoshida, Y. Verde Gomez, Carbon nanotubes as support of well dispersed platinum nanoparticles via colloidal synthesis, Journal of Power Sources, 243 (2013) 88-94.
[46] A.C. Dupuis, The catalyst in the CCVD of carbon nanotubes-a review, Progress in Materials Science, 50 (2005) 929-961.
[47] Y. Song, Q. Zhang, Y. Xu, Y. Zhang, K. Matsuoka, Z.G. Zhang, Coke accumulation and deactivation behavior of microzeolite-based Mo/HZSM-5 in the non-oxidative methane aromatization under cyclic CH4-H2 feed switch mode, Applied Catalysis A: General, 530 (2017) 12-20.
[48] Y. Xu, J. Wang, Y. Suzuki, Z.G. Zhang, Effect of transition metal additives on the catalytic stability of Mo/HZSM-5 in the methane dehydroaromatization under periodic CH 4-H2 switch operation at 1073 K, Applied Catalysis A: General, 409-410 (2011) 181-193.
[49] A.C. Ferrari, Raman spectroscopy of graphene and graphite: Disorder, electron-phonon coupling, doping and nonadiabatic effects, Solid State Communications, 143 (2007) 47-57.
[50] P. Tan, S.L. Zhang, K.T. Yue, F. Huang, Z. Shi, X. Zhou, Z. Gu, Comparative Raman Study of Carbon Nanotubes Prepared by D.C. Arc Discharge and Catalytic Methods, Journal of Raman Spectroscopy, 28 (1997) 369-372.
[51] A.M. Keszler, L. Nemes, S.R. Ahmad, X. Fang, Characterisation of carbon nanotube materials by Raman spectroscopy and microscopy - A case study of multiwalled and singlewalled samples, Journal of Optoelectronics and Advanced Materials, 6 (2004) 1269-1274.
[52] C. Castiglioni, F. Negri, M. Rigolio, G. Zerbi, Raman activation in disordered graphites of the A′ 1 symmetry forbidden k≠0 phonon: The origin of the D line, Journal of Chemical Physics, 115 (2001) 3769-3778.
[53] A. Ferrari, J. Robertson, Interpretation of Raman spectra of disordered and amorphous carbon, Physical Review B - Condensed Matter and Materials Physics, 61 (2000) 14095-14107.
[54] X. Huang, X. Jiao, M. Lin, K. Wang, L. Jia, B. Hou, D. Li, Coke distribution determines the lifespan of a hollow Mo/HZSM-5 capsule catalyst in CH4 dehydroaromatization, Catalysis Science and Technology, 8 (2018) 5753-5762.
[55] A. Adam, M.H. Suliman, M. Awwad, M.N. Siddiqui, Z.H. Yamani, M. Qamar, Controlled growth of small and uniformly dispersed Mo2C on carbon nanotubes as high performance electrocatalyst for the hydrogen evolution reaction, International Journal of Hydrogen Energy, 44 (2019) 11797-11807.
[56] M. Rahman, A. Infantes-Molina, A. Boubnov, S.R. Bare, E. Stavitski, A. Sridhar, S.J. Khatib, Increasing the catalytic stability by optimizing the formation of zeolite-supported Mo

carbide species ex situ for methane dehydroaromatization, Journal of Catalysis, 375 (2019) 314-328.
[57] W. Ding, S. Li, G.D. Meitzner, E. Iglesia, Methane conversion to aromatics on Mo/H-ZSM5: structure of molybdenum species in working catalysts, Journal of Physical Chemistry B, 105 (2001) 506-513.
[58] I. Julian, M.B. Roedern, J.L. Hueso, S. Irusta, A.K. Baden, R. Mallada, Z. Davis, J. Santamaria, Supercritical solvothermal synthesis under reducing conditions to increase stability and durability of Mo/ZSM-5 catalysts in methane dehydroaromatization, Appl. Catal. B: Environ., 263 (2020) 118360.
[59] D. Ma, Q. Zhu, Z. Wu, D. Zhou, Y. Shu, Q. Xin, Y. Xu, X. Bao, The synergic effect between Mo species and acid sites in Mo/HMCM-22 catalysts for methane aromatization, Physical Chemistry Chemical Physics, 7 (2005) 3102-3109.
[60] K. Nam, H.W. Ryu, M.Y. Gim, D.H. Kim, Enhanced reactivity and stability in methane dehydro-aromatization over Mo/HZSM-5 physically mixed with NiO, Applied Catalysis B: Environmental, 296 (2021) 120377.
[61] H.W. Ryu, K. Nam, Y.H. Lim, D.H. Kim, Effect of the NiO particle size on the activity of Mo/HZSM-5 catalyst physically mixed with NiO in methane dehydroaromatization, Catalysis Today, 411-412 (2023) 113875.
[62] L. Li, S. He, Y. Song, J. Zhao, W. Ji, C.-T. Au, Fine-tunable Ni@porous silica core–shell nanocatalysts: Synthesis, characterization, and catalytic properties in partial oxidation of methane to syngas, Journal of Catalysis, 288 (2012) 54-64.

초 록

벤젠, 톨루엔, 그리고 자일렌은 플라스틱, 고무, 직물, 약물, 그리고 페인트 등을 포함한 다양한 산업에 사용되는 필수적인 원료이다. BTX의 세계적 수요는 인구 증가, 도시화, 그리고 산업화에 따라 계속해서 증가될 것으로 예상된다. 하지만, BTX의 생산은 원유에만 크게 의존하고 있다. 메탄을 주성분으로 하는 천연가스는 그 매장량이 풍부하고 환경 친화적이어서 원유를 대체할 수 있는 좋은 탄소 공급원으로 인식되고 있다. 따라서 메탄을 이용한 BTX 생산은 경제적, 환경적으로 중요한 공정으로 평가되고 있다.

하지만, 메탄의 높은 C-H 활성화 에너지로 인해 메탄의 활용은 상당히 어려운 문제로 받아들여진다. 메탄의 전환 경로는 크게 간접 전환과 직접 전환으로 나뉜다. 간접 전환의 경우, 메탄을 먼저 수증기 개질 반응이나 부분 산화 반응 등을 통해 합성 가스(syngas)로 전환하고 이후 만들어진 합성 가스를 통해 피셔-트롭쉬 공정이나 메탄올 합성을 통해 다른 탄화수소를 생산한다. 이러한 여러 단계를 거치는 공정은 많은 에너지 소모를 유발한다. 이와 반대로, 직접 전환은 합성 가스 생산 공정 없이 메탄을 전환시켜 에너지나 경제적으로 모두 이점을 지닐 수 있다. 이러한 직접 전환은 산화 반응과 비산화 반응으로 나뉠 수 있다.

산화 반응은 메탄의 반응성을 높일 수 있지만, 대부분의 메탄이 이산화탄소와 물로 완전 산화가 진행되게 된다. 따라서, 비산화 반응이 원하는 생성물의 선택도를 높이는 가장 적절한 방법으로 받아들여지고 있다. 이러한 이유로 메탄의 탈수소 방향족화 반응(MDA)은 촉망받는 반응 중 하나이다.

Mo/HZSM-5는 MDA를 진행하는 대표적 촉매로 알려져있지만 낮은 활성과 급속한 비활성화가 극복해야할 과제로 남아있다. 이러한 촉매의 활성을 증대시키기 위해 NiO를 Mo/HZSM-5와 물리적으로 혼합하여 방향족 화합물(벤젠과 톨루엔)의 수율과 촉매의 안정성을 눈에 띄게 향상시켰다. 또한, 추가적으로 NiO와 NiO/SiO_2에 실리카 쉘을 도입하여 $NiO@SiO_2$와 $SiO_2@NiO/SiO_2$를 물리적으로 혼합하여 추가적인 증대 효과를 볼 수 있었다. X선 회절(X-ray diffraction, XRD), 메탄 승온 표면 반응(CH_4-TPSR), CO 화학 흡착, 에너지 분산 분광법을 포하한 투과 전자 현미경법(TEM-EDS), 승온 산화 반응(TPO), 라만 분광법(visible Raman), 그리고 질소 흡탈착 분석을 통해 물리적으로 혼합된 NiO가 활성점인 몰리브데넘 카바이드(MoCx) 종의 분산도를 증대시키고 코크 전구체를 자체적으로 탄소 나노 튜브(carbon nanotube, CNT)로 전환하여 MoCx에 코크가 침적되는 것을 억제한다는 것을 확인할 수 있었다. 그 결과, 반응 후 기공의

크기와 부피가 비교적 많이 유지될 수 있도록 하여 안정성 향상에 기여한다는 것을 확인하였다.

추가적으로, NiO에 실리카 쉘을 도입하여 MoCx로의 활성화 온도를 바꾸어 MoCx의 분산도를 증대시킬 수 있다는 것을 확인하였으나, 쉘은 부서졌으며 이는 쉘이 없는 NiO와 유사하게 CNT가 형성되는 결과를 가져오는 것 또한 확인할 수 있었다. NiO/SiO_2에 실리카 쉘을 도입한 경우, MoCx의 활성화 온도를 낮추어 촉매의 활성이 증대되는 것을 확인할 수 있었다. 반면, 반응 중 형성되는 Ni금속종이 NiO를 물리적으로 혼합한 경우와 달리 많이 노출되지 않아 CNT 형성이 적어 다른 비활성화 경향을 보였다. 결론적으로 본 연구에서는 NiO의 물리적 혼합과 NiO에 실리카 쉘을 도입하여 활성의 증대를 확인할 수 있었고 이를 통해서 이러한 종들이 MDA 반응에서 좋은 조촉매임을 알 수 있었다.

주요어: 메탄 탈수소방향족화 반응, 몰리브데넘 기반 촉매, 산화 니켈, 물리적 혼합, 실리카 쉘

학번: 2016-21024